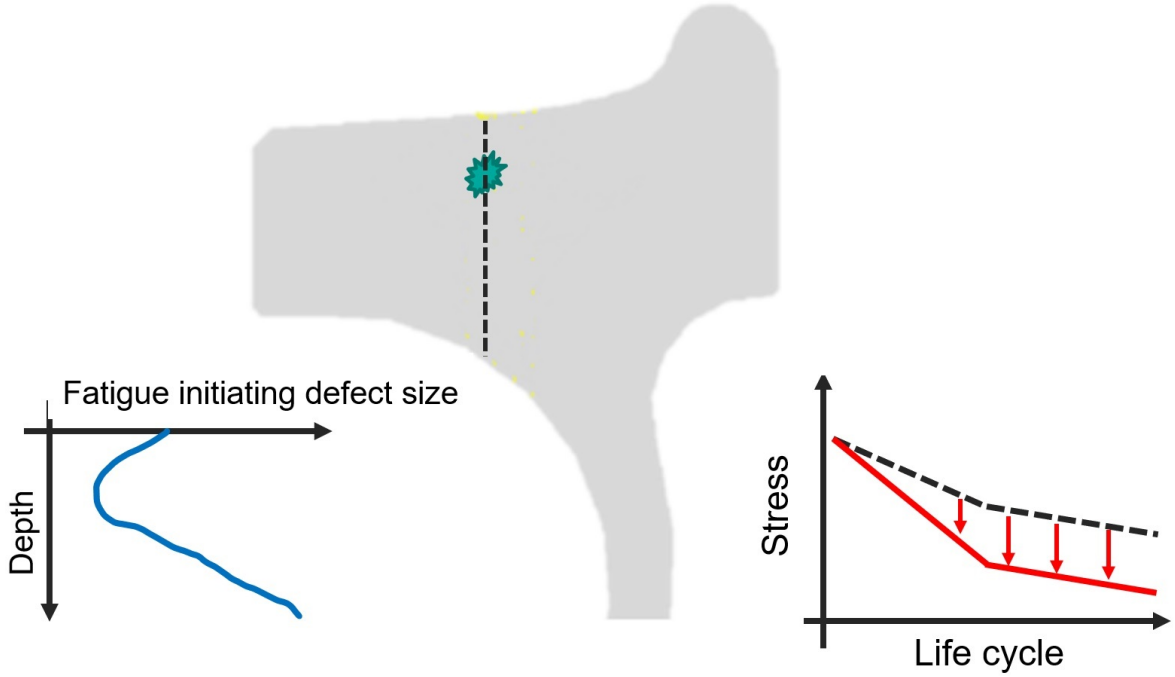

Influence of small wheel defects on the risk of subsurface-initiated rolling contact fatigue of railway wheels

Master's thesis in Mobility Engineering

JASEUNG LEE

DEPARTMENT OF MECHANCIS AND MARITIME SCIENCES

CHALMERS UNIVERSITY OF TECHNOLOGY
Gothenburg, Sweden 2023
www.chalmers.se

Master's thesis 2023

Influence of small wheel defects on the risk of subsurface-initiated rolling contact fatigue of railway wheels

JASEUNG LEE

CHALMERS
UNIVERSITY OF TECHNOLOGY

Department of Mechanics and Maritime Sciences
Division of Dynamics
Center of Excellence CHARMEC
Chalmers University of Technology
Gothenburg, Sweden 2023

Influence of small wheel defects on the risk of subsurface-initiated rolling contact fatigue of railway wheels
JASEUNG LEE

Supervisors:
Pär Söderstrom, SJ AB
Per Wessling, SJ AB
Anders Ekberg, CHARMEC

Examiner: Anders Ekberg, CHARMEC

Master's Thesis 2023
Department of Mechanics and Maritime Sciences
Division of Dynamics
Centre of Excellence CHARMEC (CHAlmers Railway MEChanics)
Chalmers University of Technology
SE-412 96 Gothenburg
Telephone +46 31 772 1000

Cover: A small defect under wheel tread and its influence on subsurface-initiated rolling contact fatigue of railway wheels.

Typeset in LaTeX
Printed by Chalmers Reproservice
Gothenburg, Sweden 2023

Influence of small wheel defects on the risk of subsurface-initiated rolling contact fatigue of railway wheels
Master's thesis in Mobility Engineering
JASEUNG LEE
Department of Mechanics and Maritime Sciences
CHARMEC
Chalmers University of Technology

Abstract

Due to improved quality control in wheel manufacturing and maintenance actions in railway operations, subsurface-initiated rolling contact fatigue rarely occurs these days. However, in some cases, fatigue poses a risk to trigger accidents such as derailments. Therefore, it requires careful monitoring in wheel maintenance.

The thesis employed Finite Element simulation (FE-simulation) and impact loads from wheel impact load detectors to study subsurface-initiated rolling contact fatigue. First, the influence of finite boundary effects on the subsurface stress field was studied by comparing stress evaluations from elastic Finite Element simulations with the analytical solutions for semi-infinite bodies. The study included an investigation of the lateral contact load position. It demonstrated that the finite boundary effects from the finite wheel body and laterally shifted contacts were insignificant.

Second, the fatigue initiating defect sizes along depths were estimated using the Dang Van multiaxial criterion and Murakami's theory. The estimation derived the Dang Van equivalent stress along depths with two cases, (1) extreme load and (2) wheel impact loads corresponding to wheel impact load detector measurements. It was found that a wheel defect at the depth from 1 to 10 mm below the wheel tread would more likely initiate subsurface rolling contact fatigue. The minimum fatigue initiating defect size (the critical defect size) occurred at depths $3 \sim 4$ mm beneath the wheel tread in both cases. The critical defect size was around 1.2 mm and 2.9 mm in each load case with non-detrimental defect size, $d_o = 40$ μm.

Finally, the thesis estimated the fatigue life of a wheel containing a defect at a depth of 6 mm from the peak and mean impact loads measurements. The estimation derived a reduced equivalent Dang Van Wöhler curve (often called SN curve) due to material defects. The reasonable fatigue life estimates were around 191×10^3 and 330×10^3 km for a defect size 1 mm and non-detrimental defect size, $d_o = 40$ μm.

The thesis confirmed the influence of a small defect (defect size of less than 1 mm) on subsurface-initiated rolling contact fatigue with given realistic impact loads. However, the analysis results were highly dependent on non-detrimental defect size, d_o, equivalent fatigue limit, σ_{eDV}, and fatigue limit cycle, N_{e}. Therefore, it needs reliable sources for the selection of fatigue properties and durable assumptions to obtain more accurate results.

Keywords: Railway wheels, subsurface-initiated rolling contact fatigue, wheel defect, Dang Van criterion, Murakami's condition.

Acknowledgements

Firstly, I would like to express my sincere gratitude to Professor Anders Ekberg from Chalmers University of Technology for his guidance and support. He always appreciated my ideas and gave thorough comments on the subject as well as suggestions for the thesis paper. He motivated me to have academic interests in fatigue mechanisms, specially multiaxial fatigue. His feedback on the FE-simulation was very crucial to find errors and fixing results.

I would like to thank Pär Södestrom and Per Wessling from SJ AB, who enthusiastically joined the weekly meetings for the past five months. Thanks to their provision of the thesis topic, we had constructive discussions in meetings. Without their help, it would have been impossible to effectively comprehend real railway operations and maintenance actions. Their active engagements and hands-on experiences contributed to the practicality of the thesis.

I also would like to also extend my appreciation to my dear friend Hon Lam Cheung, who has helped me to set up the FE-simulation. His background knowledge and advice have enabled me to run a FE-simulation using ABAQUS software.

Lastly, I would like to thank my wife, Dasom Kim, and my family in South Korea for their kind support and heartfelt prayers during the Master's program.

Jaseung Lee, Gothenburg, June 2023

Contents

1
Introduction

This chapter covers the basic theories of subsurface-initiated rolling contact fatigue (RCF) in railway wheels. It is followed by objectives and methodologies used for investigations of subsurface-initiated rolling contact fatigue. The chapter concludes with research limitations and an outline of the remaining parts of the thesis.

1.1 Background

Fatigue is a major phenomenon that must be considered in long-term railway maintenance. Rolling stock, especially railway wheels is one of the parts that are subject to fatigue. In particular, high-magnitude normal contact stresses will promote subsurface-initiated rolling contact fatigue in wheels [1].

Subsurface-initiated rolling contact fatigue of railway wheels is a critical form of deterioration that requires consideration (See Figure 1.1). Since it begins beneath the wheel surface, it is hard to detect and monitor. Conventional detection devices using ultrasonic waves also have limitations in fully detecting fatigue progression. Subsurface-initiated fatigue has been reduced as a result of improved wheel material and railway track quality. However, it is still a potentially dangerous phenomenon that, if not properly maintained, can result in a catastrophic accident such as a wheel fracture and derailment [2]. To avoid accidents, it is critical to make informed wheel maintenance decisions based on a thorough understanding of subsurface-initiated rolling contact fatigue.

Rolling contact fatigue initiated under the wheel surface is influenced by contact force-induced stress and wheel defects beneath the wheel surface. To make effective maintenance action, it is necessary to investigate how these effects influence the fatigue risk. With an assumption of semi-infinite bodies, the stress field under the contact surface can be analytically derived. Since the actual wheel has finite boundaries, however, the analytical solution may not accurately evaluate the stress field near to the wheel side [3]. Finite Element simulations can be a useful tool for studying the boundary effects on stress/strain field.

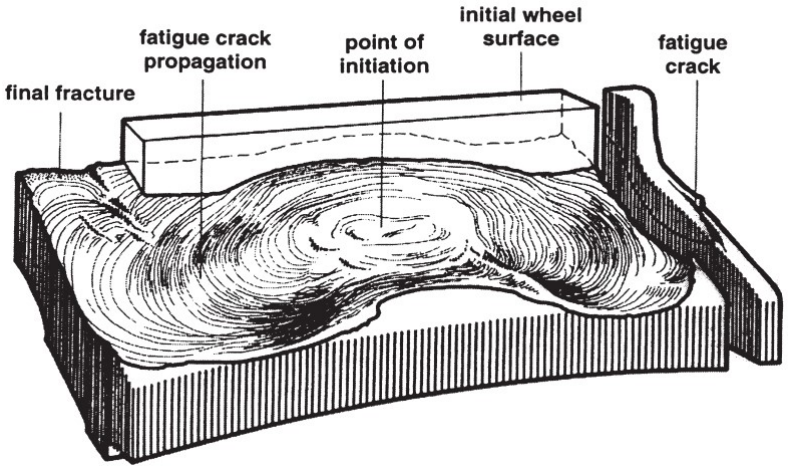

Figure 1.1: Sketch of the subsurface-initiated crack on a railway wheel. From [4].

1.2 Objective

The main aims are to comprehend the influence of (1) finite boundary and (2) wheel defect sizes on the risk of subsurface-initiated rolling contact fatigue. The thesis aims to provide input to the wheel reprofiling on the risk of subsurface-initiated RCF.

1.3 Methodology

- Study the influence of boundary conditions on subsurface stress field, and thereby on subsurface-initiated rolling contact fatigue. To this end, stresses derived from Finite Element simulations are compared to analytical solutions for semi-infinite bodies

- Extend simulations to investigate influence of reprofiling and lateral contact load position

- Estimate the influence of defect size on fatigue strength based on Murakami's theory

- Extend to 3D analysis to evaluate Dang Van stress, establishing an equivalent Dang Van Wöhler curve, considering the influence of subsurface material defect sizes and load spectra

1.4 Research limitation

- Wheel profile of the S1002 trailer wheel used in the Finite Element simulation does not exactly match the profile mounted in the considered railway vehicle

for which the load spectra were derived. Numerical errors from minor geometric differences between the simulation and the actual wheel are ignored

- Influence of lateral load on subsurface initiated rolling contact fatigue is assumed to be small and will not be considered

- A wheel model in Finite Element simulation only considers a linear elasticity of the material. The plasticity effect on stress distribution under wheel tread and fatigue initiation is not considered in the simulation.

1.5 Thesis outline

The present thesis is followed by four chapters. Chapter 2 introduces relevant theories of rolling contact mechanics and multiaxial fatigue. Chapter 3 explains how to build railway wheel model and evaluate finite boundary effects in FE-simulation. This chapter also presents procedures to estimate fatigue initiating defect sizes and fatigue life using FE-simulation and WILD measurements. Chapter 4 presents FE-simulation results for analyzing effects of finite boundary and defect sizes on subsurface-initiated RCF. Estimating fatigue initiating defect sizes and fatigue life from wheel impact load measurements are also discussed. The conclusions and future works are presented in Chapter 5.

2

Theory

2.1 Rolling contacts

2.1.1 Hertzian contact stresses

When a railway wheel rolls on the rail, it contacts in a small patch. In the small contact area, rolling contact between railway wheels and rails can be approximated as a contact between two cylinders [5]. Assuming that both wheel and rail feature linear elastic material, a smooth geometry, and are semi-infinite, the contact patch has an elliptical shape, see Figure 2.1. In that case, the contact pressure distribution can be expressed as

$$p(x,y) = p_o\sqrt{1 - \frac{x^2}{a^2} - \frac{y^2}{b^2}} \tag{2.1}$$

where x and y are defined as coordinate systems in the rolling and transverse direction from the center of the contact patch, a and b are contact semi-axes of the contact patch, p_o is the maximum contact pressure that is evaluated from the normal load P as

$$p_o = \frac{3}{2}\frac{P}{\pi ab} \tag{2.2}$$

Contact semi-axes a and b can be determined from material properties and geometric parameters, i.e. Young's Modulus and Poisson's ratio, wheel and rail radius, and wheel axle load (See chapter 13 of the [6] for a detailed derivation).

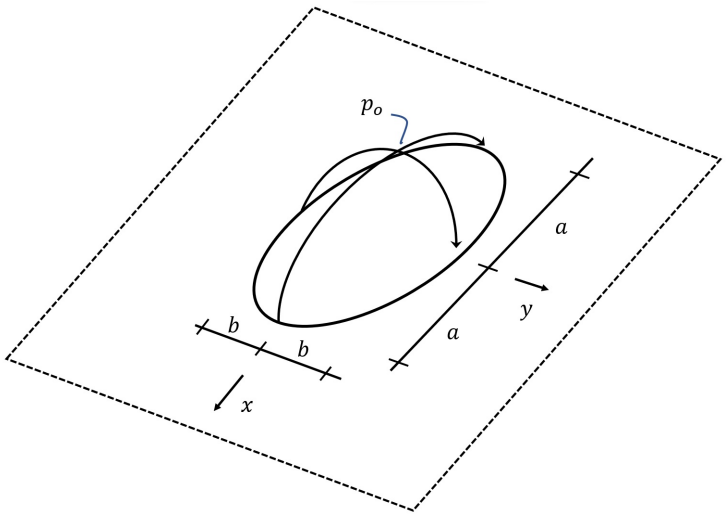

Figure 2.1: Hertzian contact pressure distribution with maximum contact pressure, p_o, and semi-axes a and b

2.1.2 Finite boundary effects

Analytical solutions provides the stress distribution under elastic contact conditions of semi-infinite bodies [7]. This analytical solution derives the deformation equations in elastic contact, and computes strains and stress based on this calculated deformation (See the appendix of [7] for a detailed derivation).

Since the real railway wheel has a finite-boundaries, the analytical solutions can have limitations in describing stress distribution close to boundaries [3]. Finite Element (FE) based approaches can be used to account for the boundary effects on the stress distribution and thereby on subsurface fatigue initiation of railway wheels.

2.2 Multiaxial fatigue

2.2.1 Stress-based model

Including railway wheels, most materials in rolling components experience multiaxial loads such as bending and torsion. There have been many studies to understand mechanisms and estimate the fatigue strength of materials subject to multiaxial loads. Stress-based models attempt to derive multiaxial fatigue criteria based on stress states in material. Typically, they define equivalent stresses representative of the fatigue impact under multiaxial loading conditions.

A key concept in stress-based models is the critical plane approach. This implies that there is a particular material plane where the fatigue impact becomes highest in the material point under the multiaxial load. Multiaxial fatigue criteria typically assume that fatigue initiates in such a critical plane. There are various types of multiaxial fatigue criteria, e.g., Findley, McDiarmid, and Dang Van [8]. These models have common philosophies: All models use shear stress and normal stress to derive an

equivalent stress. However, they employ different interpretations in defining shear stress, normal stress, and critical planes (See chapter 5 of [8] for details).

2.2.2 Dang Van criterion

The Dang Van criterion is one of the most commonly used multiaxial fatigue criterion in rolling contact fatigue. The Dang Van criterion evaluates fatigue initiation by projecting the stress-time series on a critical plane. The criterion exploits two empirical facts explained below [12].

The first fact is that shear stress amplitude (deviation of the shear stress from its mid value during a stress cycle) mainly contributes to fatigue initiation. If the magnitude of the static shear stress is not high enough for generating global plasticity, static shear stress provides no effect on fatigue initiation. The second fact is that a tensile hydrostatic stress promotes fatigue initiation. On the other hand, a compressive hydrostatic stress can enhance fatigue strength up to a certain limit.

The Dang Van stress represents a time-dependent state of stress using the shear stress amplitude, $\tau_{\mathrm{a}}(t)$, the hydrostatic stress, $\sigma_{\mathrm{h}}(t)$, the equivalent fatigue limit of the Dang Van criterion, σ_{eDV}, and a material parameter, c_{DV} as below.

$$\sigma_{\mathrm{EQ,DV}} = \max_{t} \left(\tau_{\mathrm{a}}(t) \; + \; c_{\mathrm{DV}} \, \sigma_{\mathrm{h}}(t)\right) > \sigma_{\mathrm{eDV}} \tag{2.3}$$

The shear amplitude, $\tau_{\mathrm{a}}(t)$ is evaluated as the difference between the mid value of the shear stress during a load cycle, and the current value of shear stress, i.e, $\tau_{\mathrm{a}}(t) = \tau(t) - \tau_{\mathrm{mid}}(t)$, see Figure 2.2 and the appendix of [4] for details.

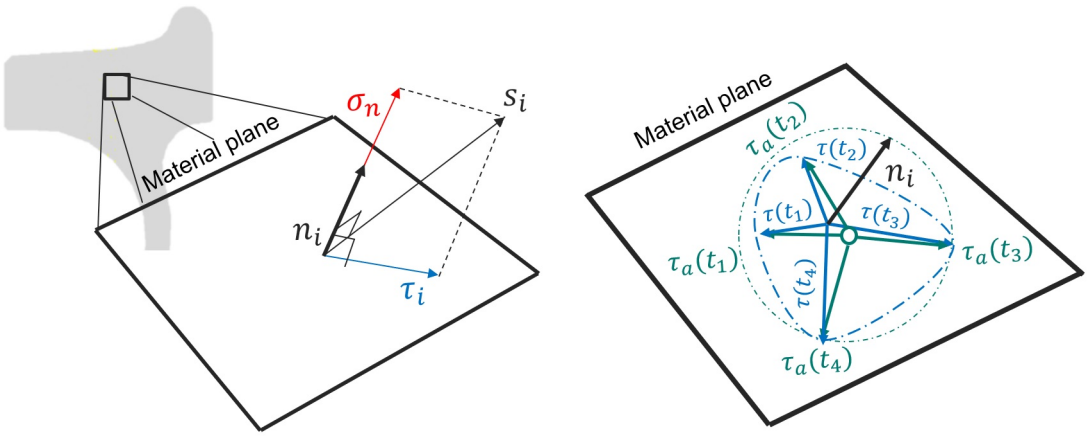

Figure 2.2: Shear amplitude, $\tau_{\mathrm{a}}(t)$ from shear stress path, $\tau(t)$ in a material plane

The Dang Van criterion views the fatigue process on a microscale (often called mesoscale). In this criterion perspective, fatigue initiates when the load magnitude exceeds the elastic shakedown limit at the microscale. During the elastic shakedown, local stresses induce plastic deformation and microscopic residual stress. The Dang

Van criterion quantifies those microscopic fatigue behaviours as local shear stress and local hydrostatic stress on the critical plane [9] – [10].

2.3 Material defect effects: Murakami's theory

Despite improvements in the quality of railway wheel manufacturing technology, it is difficult for wheels to fully avoid material defects in the manufacturing process. Small defects and inclusions in the material can influence the fatigue limit and threshold stress for non-propagating cracks, see Figure 2.3.

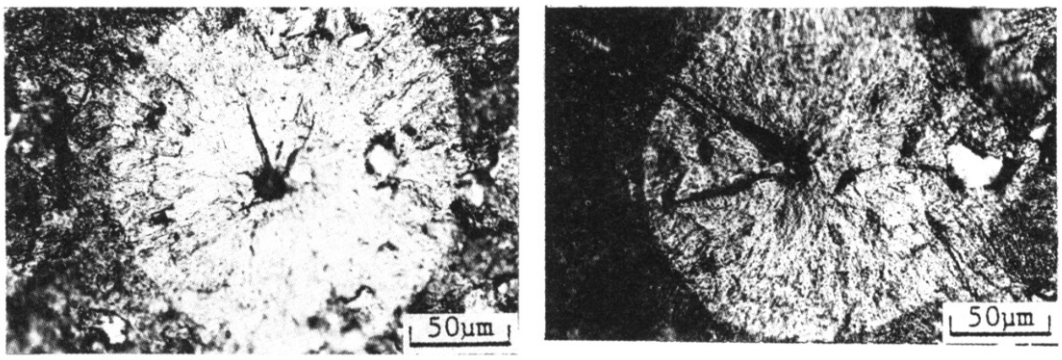

Figure 2.3: Typical example of material inclusions, fisheye. From [11]

Murakami's criterion is one of the most commonly used approaches to evaluate reduced fatigue strength in the presence of small material defects. Murakami empirically studied how small defects (grain level size) affected the fatigue limit of metallic materials [2].

By assuming material defects to be circular when projected on the critical plane, a reduced fatigue limit can be derived as

$$\sigma_{\mathrm{eDV,red}} \simeq \sigma_{\mathrm{eDV}} \left(\frac{d}{d_o} \right)^{-\frac{1}{6}} \tag{2.4}$$

where $\sigma_{\mathrm{eDV,red}}$ is the fatigue limit reduced due to a material defect size of d, and d_o is the defect size corresponding to fatigue initiation at a stress magnitude σ_{eDV} [3]. Fatigue initiation of railway wheels containing defects can be assessed by the criterion.

$$\sigma_{\mathrm{EQ,DV}} > \sigma_{\mathrm{eDV,red}} \tag{2.5}$$

2.4 Residual stress effects

Heat treatment is one of key processing for hardening railway wheels during the manufacturing process. Quenching is one of the most commonly used heat treatment process as shown in Figure 2.4. It consists of spraying cooling liquids onto

the rims of heated railway wheels. By quenching, railway wheels obtain hardening zones with compressive residual stresses beneath wheel flanges and treads [14] (See Figure 2.5).

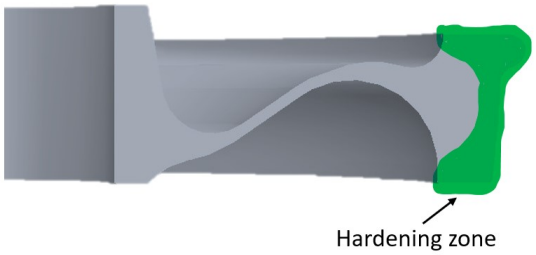

Figure 2.4: Hardening zone from heat treatment by wheel quenching

Since compressive stresses help closing cracks in the materials, the compressive residual stresses induced by heat treatment improve the fatigue strength of the wheels. A static shear stress will not affect $\sigma_{\mathrm{EQ,DV,res}}$. Thus, the Dang Van criterion can consider the residual stress effects on fatigue initiation using a term, $\sigma_{\mathrm{h,res}}$ as (2.6).

$$\sigma_{\mathrm{EQ,DV,res}} = \sigma_{\mathrm{EQ,DV}} + c_{\mathrm{DV}} \frac{\sigma_{\mathrm{h,res}}}{3} > \sigma_{\mathrm{eDV}} \tag{2.6}$$

where tensile residual stresses are positive.

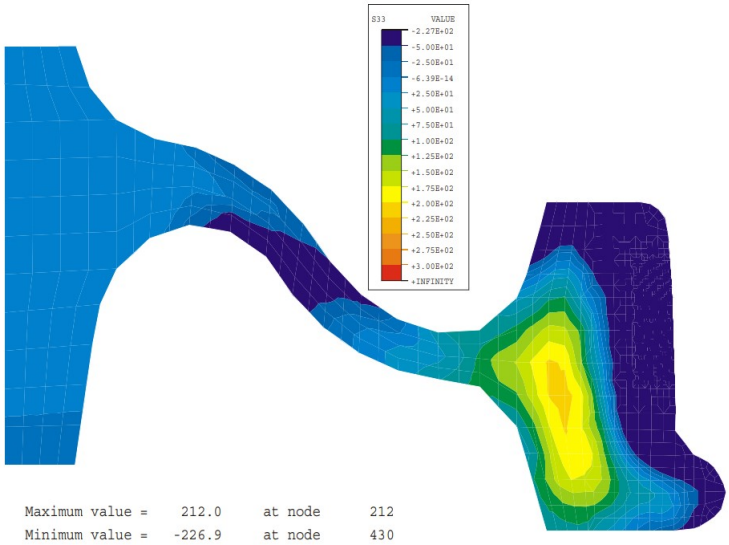

Figure 2.5: Hoop residual stress in a radial section of a manufactured wheel. From [15]

2.5 Fatigue life: Wöhler curve

The Wöhler curve (often called SN curve) describes the relation between a cyclic load (stress amplitude) and the resulting fatigue life (number of cycles) of the material. The curve is normally estimated from fatigue testing in uniaxial loading. It often shows linear characteristics for metallic materials in log-log scales for fatigue lives in the range 10^3 – 10^6 cycles (See Figure 2.6).

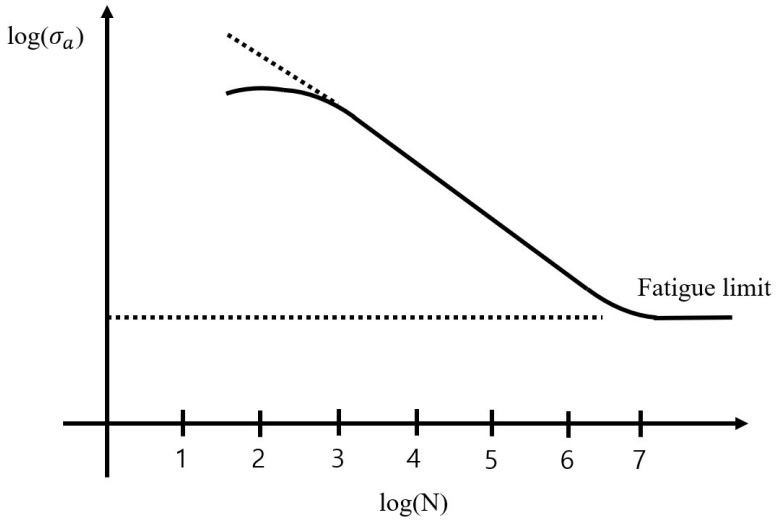

Figure 2.6: Wöhler curve (SN curve)

The Wöhler curve can be modified to account for the effects of various factors that affect the fatigue resistance. This includes mid stresses, surface conditions, stress concentrations, and material defects. Therefore, the Wöhler curve can be employed as a fundamental tool to predict fatigue life under uniaxial loading.

For the current study, the Wöhler curve is modified to account for the multiaxial loading by employing the Dang Van equivalnet stress. In addition, the fatigue limit is decreased based on Murakami's theory (See Figure 2.7).

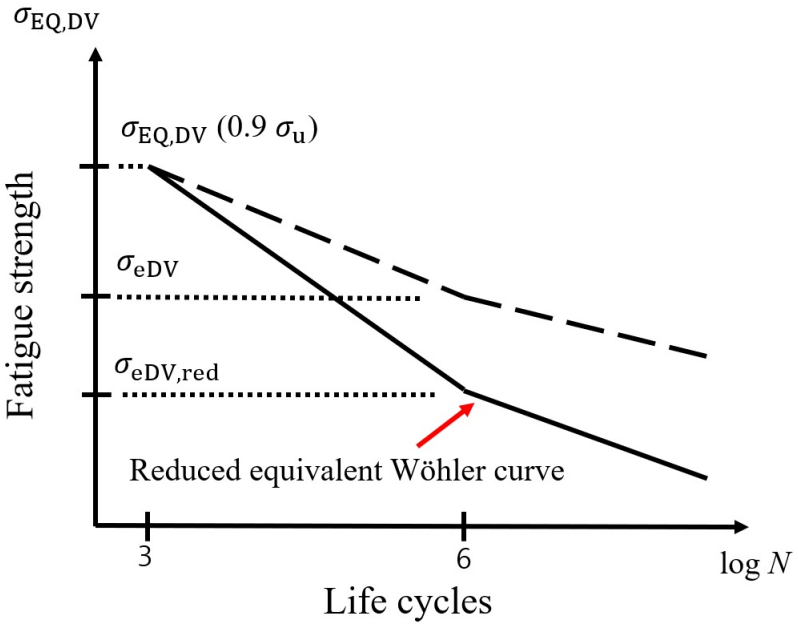

Figure 2.7: Equivalent Wöhler curve with fatigue limit reduction

3
Methodologies

3.1 Railway wheel model

3.1.1 Model construction

The draft of an X2 trailer wheel was obtained from SJ AB. A 3D wheel model was constructed using the software, ABAQUS. Since the whole wheel model is too computationally heavy, the model features a wheel sector covering 20 degrees around the contact patch, see Figure 3.1.

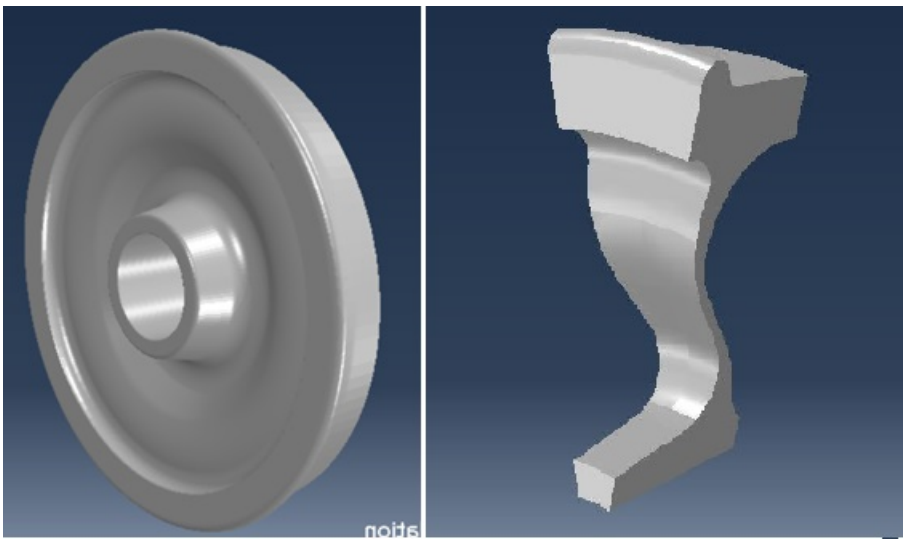

Figure 3.1: X2 trailer wheel model in ABAQUS, entire wheel model (left) and a partial model (right)

3.1.1.1 Loading condition

The model employs moving Hertzian contact loads. Contact pressure between the rail and wheel forms the Hertzian contact pressure, which implicitly pressumes that loads induced by friction between wheel and rail do not have a significant influence on subsurface-initiated fatigue [3]. Figure 3.2 illustrates the contact pressure load applied on the partial wheel model.

Table 3.1 lists contact patch dimension and maximum contact pressure for different axle loads. Input parameters used for the calculations are Young's Modulus,

$E = 210$ GPa, Poisson's ratio, $\nu = 0.3$, wheel, and rail radius, $R_1 = 0.442$ m, and $R_2 = 0.3$ m.

Table 3.1: Semi-axis of contact patches and maximum contact pressure with axle loads from 18 to 30 tonnes

Axle load [tonnes]	18	20	22	24	26	28	30
a [mm]	6.8	7.0	7.3	7.5	7.7	7.9	8.0
b [mm]	5.2	5.4	5.6	5.8	5.9	6.1	6.2
p_o [GPa]	1.19	1.23	1.27	1.31	1.34	1.37	1.41

Note that actual static axle loads of X2 trailer wheels range around $12 - 15$ tonnes. However, this study employs the loads above static levels to study extreme conditions, e.g, for severely out-of-round wheels.

3.1.1.2 Boundary condition

The boundary condition for the partial model assumes that displacement and rotation of points far from the contact patch are very small or negligible. Figure 3.2 depicts the rigidly fixed boundary conditions at both end sides and on the axle side (bottom surface) of the partial wheel model.

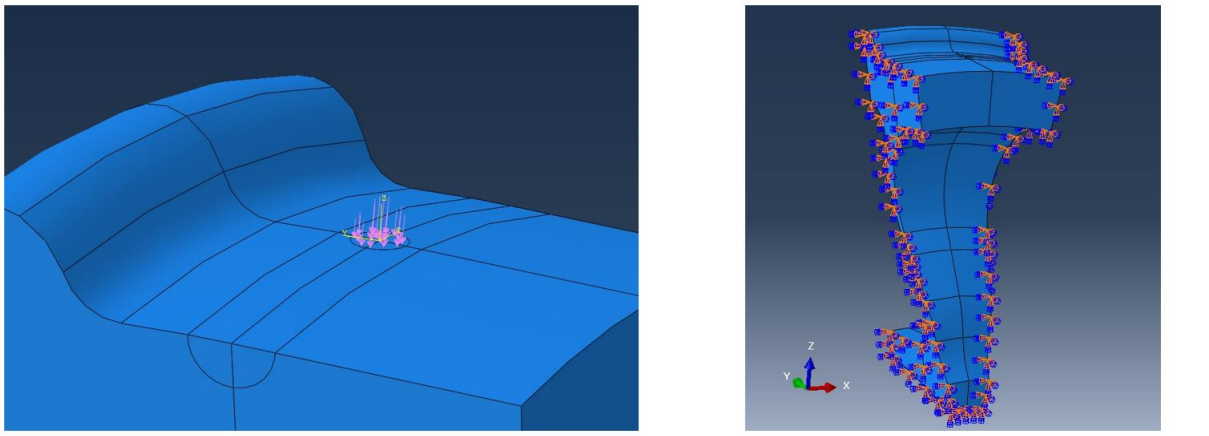

(a) Pressure load using Hertzian contact (b) Boundaries rigidly fixed at the end sides

Figure 3.2: The partial model with (a) loading condition and (b) boundary condition

3.1.2 Contact force measurement

There are wheel impact load detectors (WILD) installed on the railway track to detect damaged wheels on Swedish railway lines. Measurements show the level of maximum and average vertical contact force between wheels and rail. The SJ AB provided measurements from WILDs at a Dammstorp (near Malmö), see Figure 3.3. This study analyzes contact force measurements from detectors located at the Dammstorp.

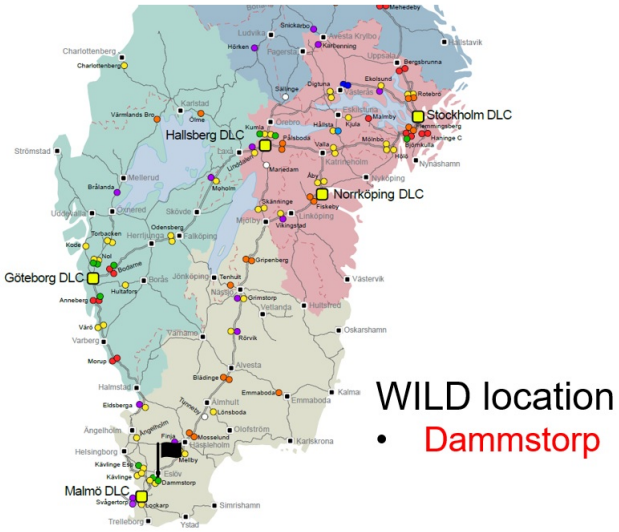

Figure 3.3: Locations of employed wheel impact load detectors (marked by black flags). Original figure from [16].

Contact forces of X2 trailer wheels are investigated. The passenger trains have static axle loads of around 12 $\sim$ 15 tonnes and pass detectors at a speed of about 100 $\sim$ 170 km/h. The contact force measurement period was 12 months from September 2020 to September 2021, see Chapter 4 for details.

3.2 Finite boundary effects

This methodology was used to study the influence of finite boundary effects on the stress distribution to compare with analytical solutions. It only includes nominal contact and contact laterally shifted contact towards the field side, see Figure 3.4. Note that both analytical solutions and FE-simulation results assume elastic conditions.

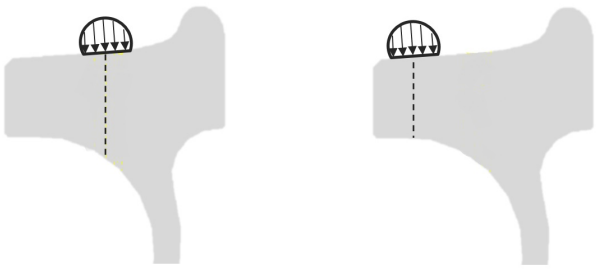

(*a*) Nominal contact (*b*) Field-side contact

Figure 3.4: Nominal and field-side contacts for the analysis of finite boundary effects

3.3 Material defect size

3.3.1 Rolling contact representation

To represent rolling contact, the contact patch is moved along the wheel tread in the circumferential direction (x in Figure 3.5). Stress distributions are evaluated at fixed depths at each contact patch position. The stress distribution in a fixed point represents the stress history of that material point during an over-rolling. Figure 3.5 illustrates the longitudinal contact patch movement. Here, l is the contact patch's center position, ranging from -30 to 30 mm.

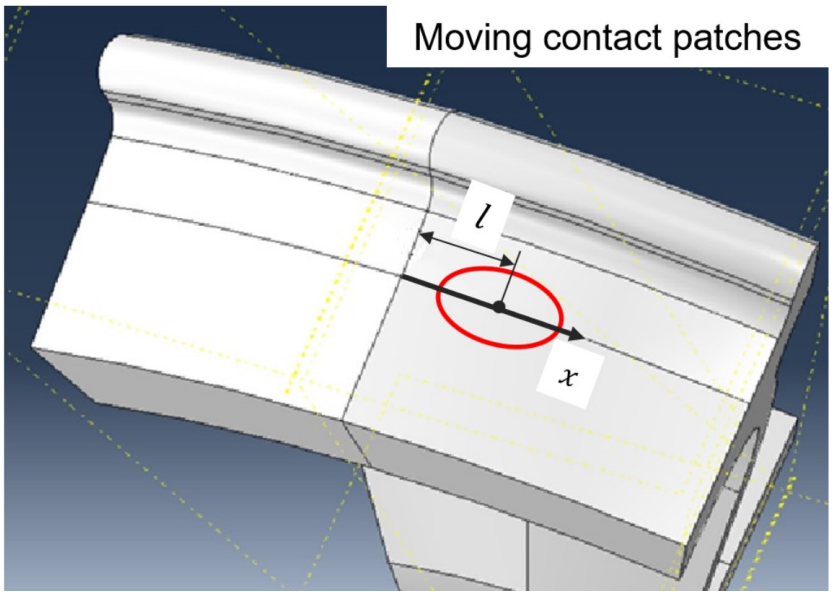

Figure 3.5: Contact patch movement on the wheel tread

This study employs the equivalent Dang Van stress to quantify the multiaxial state of stress in the rolling contact. It derives equivalent Dang Van stress using the equation (2.2) from the stress-time series obtained from FE simulations.

There are two parameters in the Dang Van criterion, c_{DV}, and σ_{eDV}. The material property, c_{DV} is assumed to be a constant with a value of 0.3 in this thesis. The fatigue limit of the Dang Van criterion, σ_{eDV} is taken as the fatigue limit in shear from experimental results in [4].

3.3.2 Fatigue initiating defect size

Based on the equation (2.4) and (2.5), a material defect size, d_{FI} which initiates subsurface rolling contact fatigue at a certain $\sigma_{\mathrm{EQ,DV}}$ magnitude can be evaluated as,

$$d_{\mathrm{FI}} = d_o \left(\frac{\sigma_{\mathrm{EQ,DV}}}{\sigma_{\mathrm{eDV}}} \right)^{-\frac{1}{6}} \tag{3.1}$$

The d_{FI} also depends on the size of the non-detrimental defect size, d_o. This calls for sensitivity analyses to enhance estimation accuracy, see Chapter 4 for details. The Murakami condition is valid when the defect size is small, which in this contaxt is less than around 1 mm. If the defect size is larger, the theory of Linear Elastic Fracture Mechanics (LEFM) is required to describe defect size effects.

3.4 Fatigue life estimation

3.4.1 Dang Van stress as a function of depth

For a more efficient evaluation of the fatigue life, a fatigue initiation index, FI_{sub} for subsurface-initiated rolling contact fatigue can be employed. FI_{sub} approximates the maximum (considering depth) Dang Van stress from contact forces of pure rolling contact (frictionless-rolling contact) as

$$\max_{z}\left(\sigma_{\mathrm{EQ,DV}}(z)\right) \approx FI_{\mathrm{sub}} = \frac{P}{4\pi ab} + c_{\mathrm{DV}}\,\sigma_{\mathrm{h,res}} \tag{3.2}$$

where P is the vertical contact force, a and b are contact patch semi-axes [21].

According to the analytical solutions [7] and FE-simulations conducted in this study, the maximum Dang Van stress normally occurs at around $3 \sim 4$ mm below the wheel tread surface and decreases at higher depths. To investigate fatigue initiation with FI_{sub}, it is observed from FE-simulations that the maximum values of shear stress and Dang Van stress follow semi-linear relations at depths from 3 mm to 11 mm. More detailed results are presented in Chapter 4.

3.4.2 Reduced Dang Van Wöhler curve considering defect sizes

The Wöhler curve described in Chapter 2 can be modified to consider material defects. One of the methods is to reduce the equivalent Wöhler curve based on Murakami's theory.

From the reduced Dang Van equivalent Wöhler curve, fatigue damage per loading cycle can be evaluated. By linear accumulation, the railway wheel operating distance can be estimated, see Chapter 10 of [13] for more details. Figure 3.6 illustrates the fatigue life estimation process using FI_{sub} and the reduced Dang Van equivalent Wöhler curve.

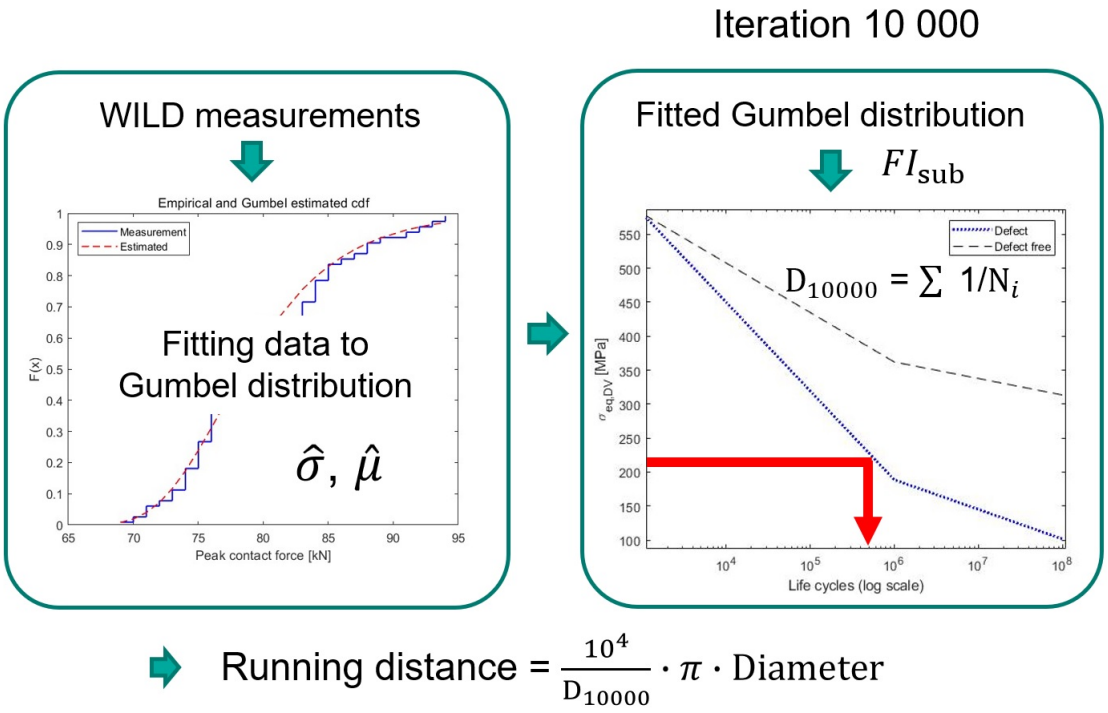

Figure 3.6: Fatigue life estimation using reduced Dang Van Wöhler curve

4

Results

This chapter covers FE-simulation results performed to investigate finite boundary effects on subsurface stress distribution and fatigue initiating defect sizes. It also includes fatigue life estimation of railway wheels containing small subsurface defects using loads from WILD measurement. The defect size analyses and wheel life estimations also feature sensitivity analyses to identify parameters dominantly contributing to the damage.

4.1 Finite boundary effects on the stress distribution along depths

This section covers nominal and laterally shifted contact positions to investigate boundary effects. The center position of the contact patch in the nominal case is 65 mm from the field side of the wheel. The lateral cases have the center of the contact at 30 mm and 15 mm from the field side of the wheel.

Finite boundary effects are evaluated by comparing the maximum shear stress distribution from FE-simulations with analytical solutions. In the FE-simulations, the Hertzian contact load is applied with maximum contact pressure $p_o = 1.41$ GPa, corresponding to an axle load of around 30 tonnes Note that this is an extreme case to provoke an effect.

Figure 4.1 shows the maximum shear stress distribution at the contact patch center point. Both FE-simulations and analytical solutions follow similar trends. The maximum shear stress increases up to a peak value at a depth of around $3 \sim 4$ mm and then decreases at deeper depths.

The FE-simulation results tend to have a higher stress level than the analytical solution. Unlike analytical solutions assuming a semi-infinite and continuous body, FE-simulation contains a finite body with numerical errors in results. This can explain the differences between the two analyses.

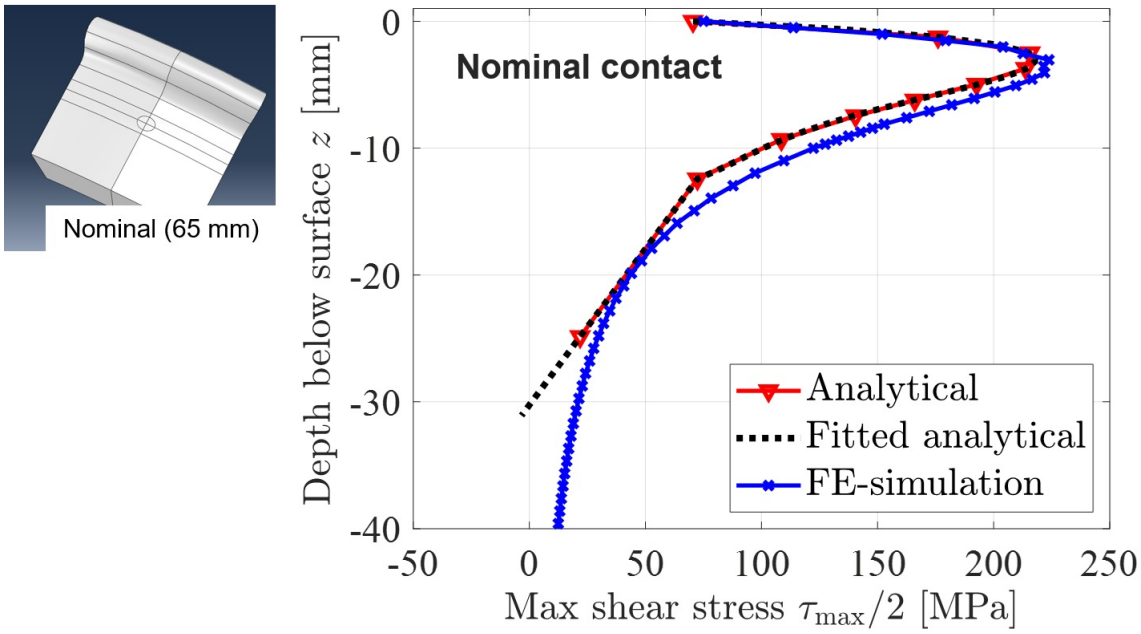

Figure 4.1: Maximum shear stress of the nominal contact case, with contact 65 mm from field side

Figure 4.2 shows results from the laterally shifted contact cases with contact, 30 mm and 15 mm from the field side. As the contact patch comes close to the edge, the maximum shear stress level increases as shown in the close-up in Figure 4.3.

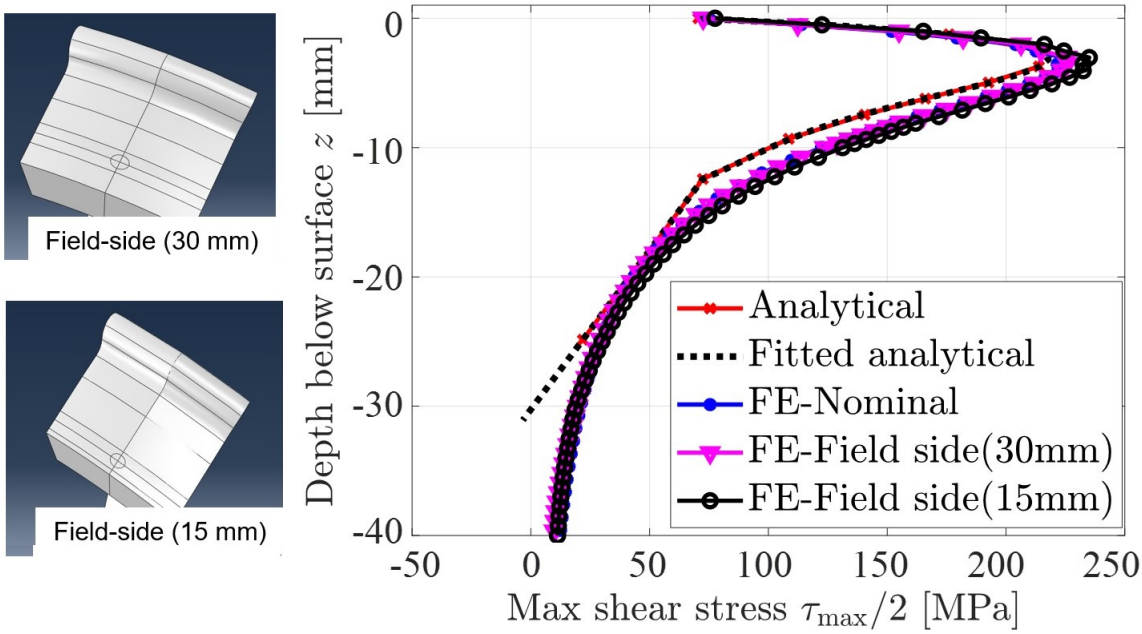

Figure 4.2: Maximum shear stress in the nominal contact and laterally shifted contacts

Since the railway wheels are capable to limit lateral contact movement by wheel flange, lateral contact is normally 30 $\sim$ 100 mm from the field side. In other words,

the lateral contact at 15 mm from the field side rarely, only occurs (An example where it can happen is when hollow worn wheels pass a crossing) Therefore, finite boundary effects on subsurface surface-initiated rolling contact fatigue can be considered to be minor.

Note that these FE-solutions do not take into account any plasticity which can occur close to free surfaces. In such cases, boundary effects will be more significant.

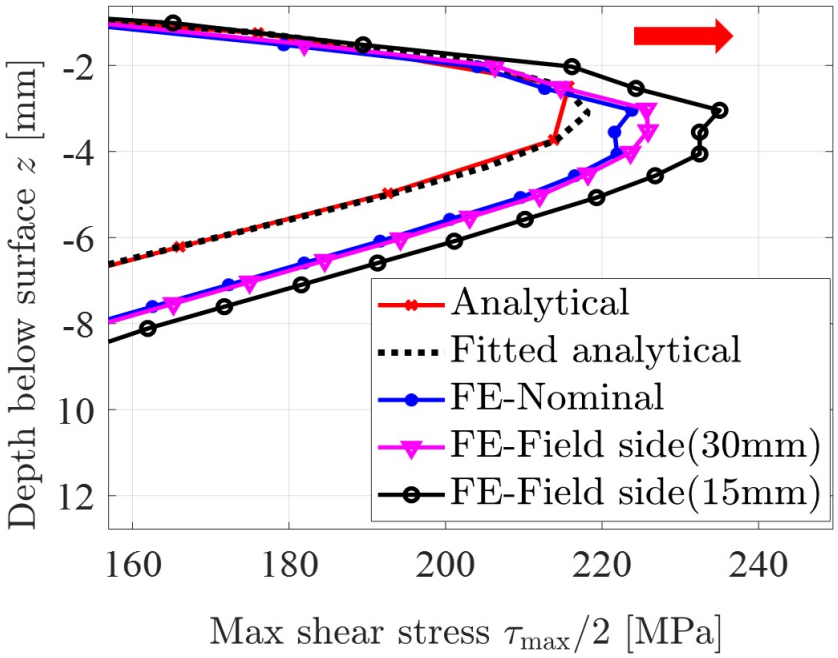

Figure 4.3: Maximum shear stress of nominal and laterally shifted contacts at depths around that of peak $\tau_{\max}/2$

4.2 Fatigue initiating defect size analysis

4.2.1 Defect size estimation with Dang Van criterion

This section analyzes fatigue-initiating defect sizes induced by rolling contact loads. By moving a contact patch in the circumferential direction, subsurface stress-time series are evaluated (See Chapter 3.3). Figure 4.4 illustrates six stress components at a depth of 3.2 mm when loaded by Herztian contact pressure, $p_o = 1.41$ GPa.

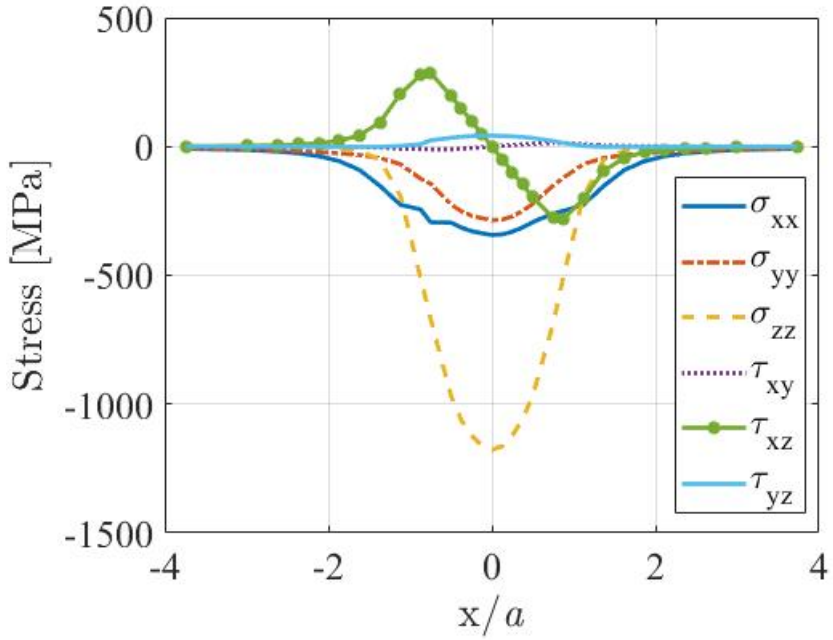

Figure 4.4: Stress distribution as function of load position at a depth, 3.2 mm

The equivalent Dang Van stress represents multiaxial loads to evaluate the risk of fatigue initiation from the obtained stress-time series. In calculating shear stress amplitude, τ_a, min-max and eigenvalue problems are required to be solved, see [12] for more details. Figure 4.5 illustrates the equivalent Dang Van stress, $\sigma_{\mathrm{EQ,DV}}$ obtained from the stress history at a depth of 3.2 mm, where the maximum $\sigma_{\mathrm{EQ,DV}}$ is around 232.2 MPa.

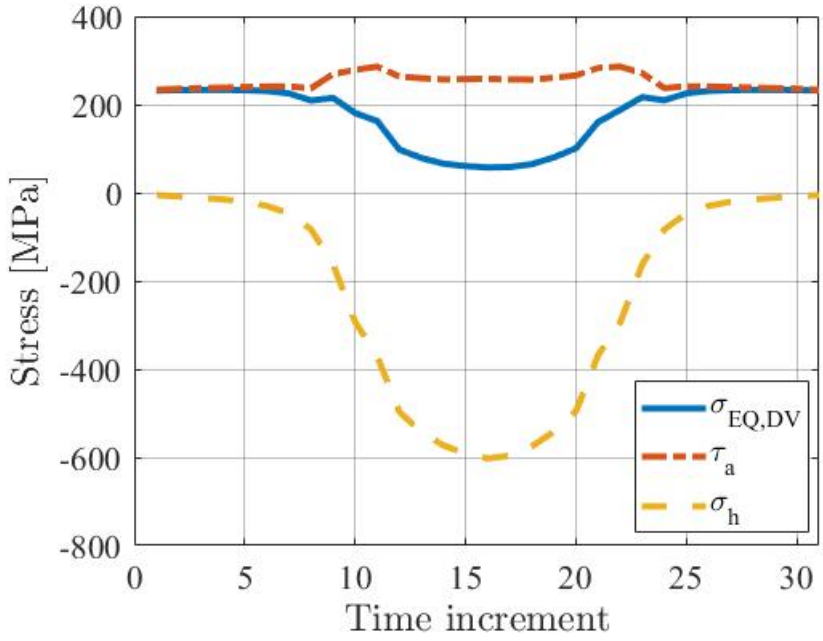

Figure 4.5: Equivalent Dang Van stress, shear stress "amplitude" and hydrostatic stress at a depth of 3.2 mm

The distribution of the maximum $\sigma_{EQ,DV}$ along the depth forms a similar pattern to the maximum shear stress along depths, see Figure 4.1 and 4.6. Since the compressive hydrostatic stress is high at shallow depths, the peak value of $\sigma_{EQ,DV}$ occurs at a depth around 4 mm, which is slightly deeper than the depth at where the maximum shear stress τ_{max} occurs.

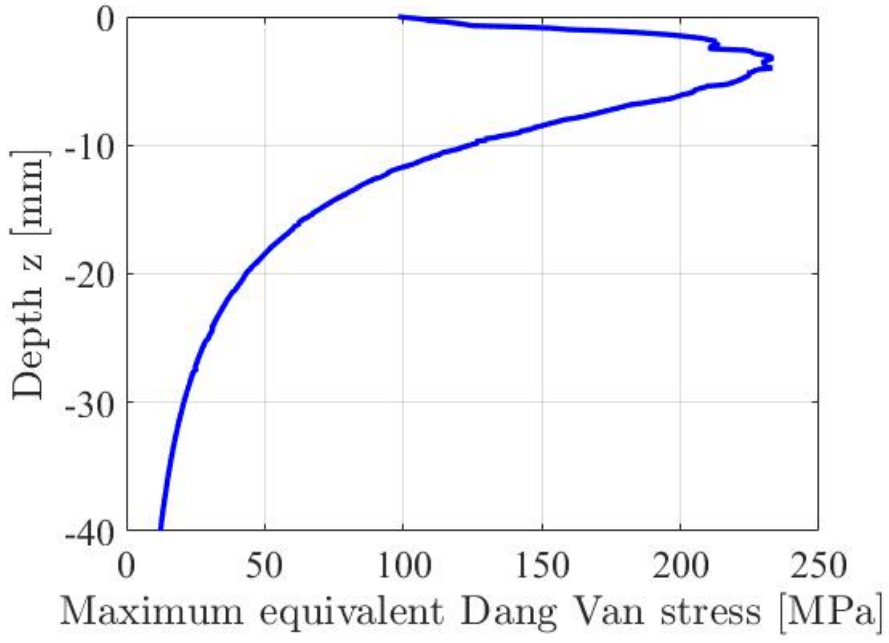

Figure 4.6: Maximum equivalent Dang Van stresses along depth at the fixed point

Based on the evaluated maximum $\sigma_{\mathrm{EQ,DV}}$, Figure 4.7 shows the corresponding fatigue initiating defect size distribution with $d_o = 20$ μm and $\sigma_{\mathrm{eDV}} = 362$ MPa. It is found that under these circumstances defect sizes less than 1 mm can initiate fatigue at depths from 1.3 mm to 6.65 mm, see the dotted line in Figure 4.7. The critical defect size, $d_{\mathrm{FI,min}}$ is 0.28 mm at the depth of 3.2 mm where the $\sigma_{\mathrm{EQ,DV}}$ has a peak value.

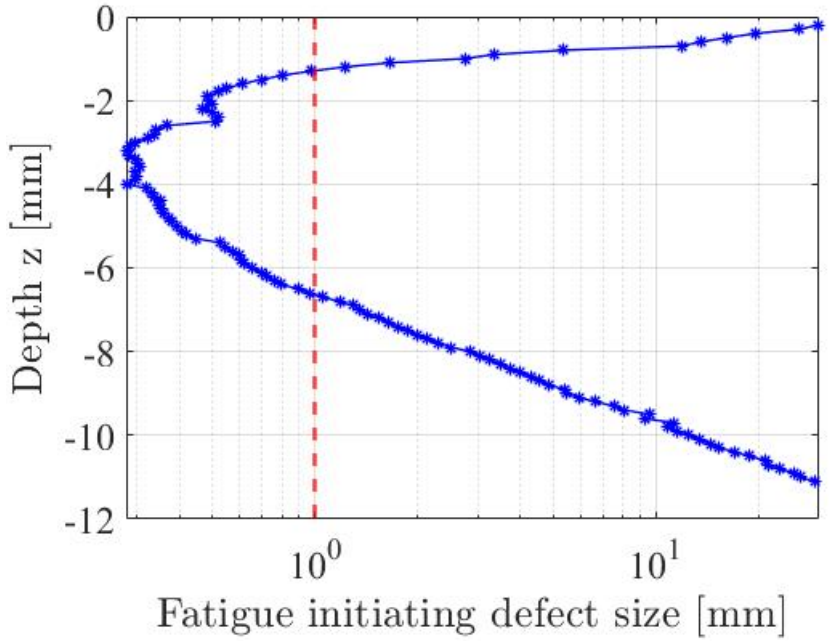

Figure 4.7: Defect size causing subsurface RCF along depths for $d_o = 20$ μm and $\sigma_{\mathrm{eDV}} = 362$ MPa

4.2.2 Residual stress effects

The equivalent Dang Van stress can consider residual stress effects induced by heat treatment (See equation (2.6)). The thesis applied approximated hoop residual stresses from [17], see Figure 4.8. In Figure 4.8, the measured residual stress (dotted line with red color) is the average stress over the wheel rim thickness below the wheel tread using ultrasonic devices. Simulation results (blue line) were obtained from simulations using an elastic plastic model with creep effects, see [17] for more details.

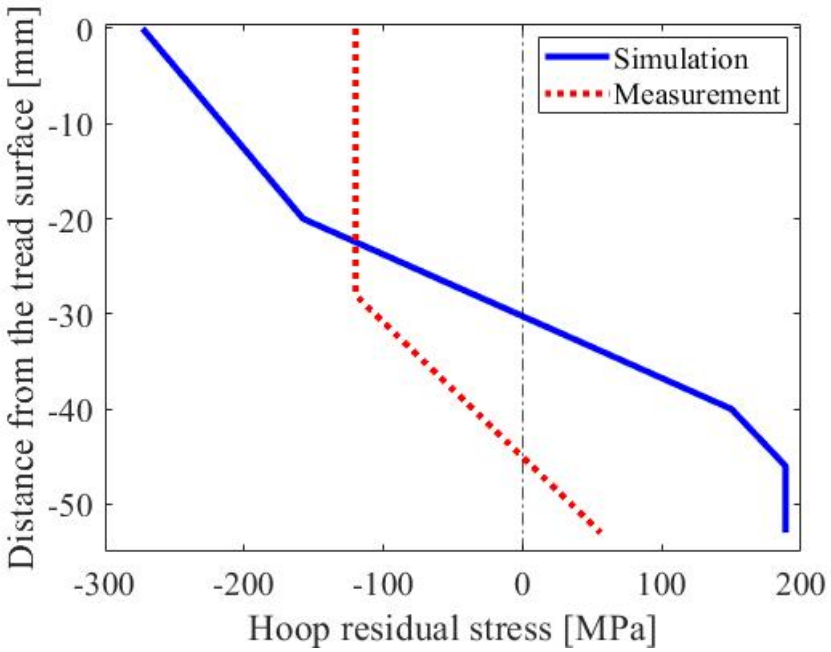

Figure 4.8: Hoop residual stresses along depth approximated from [17]

At depths where hoop residual stresses are compressive, they reduce the equivalent Dang Van, see Figure 4.9. As depth becomes deeper than some $20 \sim 40$ mm, tensile hoop residual stresses cause increased equivalent Dang Van stresses.

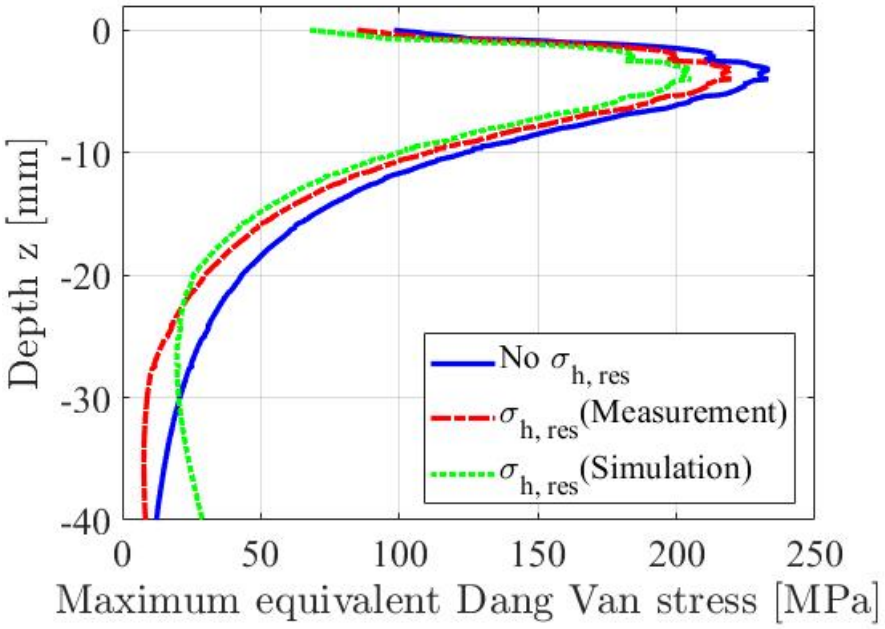

Figure 4.9: Maximum equivalent Dang Van stress along depth with residual stress effects

Reduced Dang Van stresses from compressive hoop residual stresses result in in-

creasing fatigue initiating defect sizes, see Figure 4.10. This will increase the critical defect size, see Table 4.1.

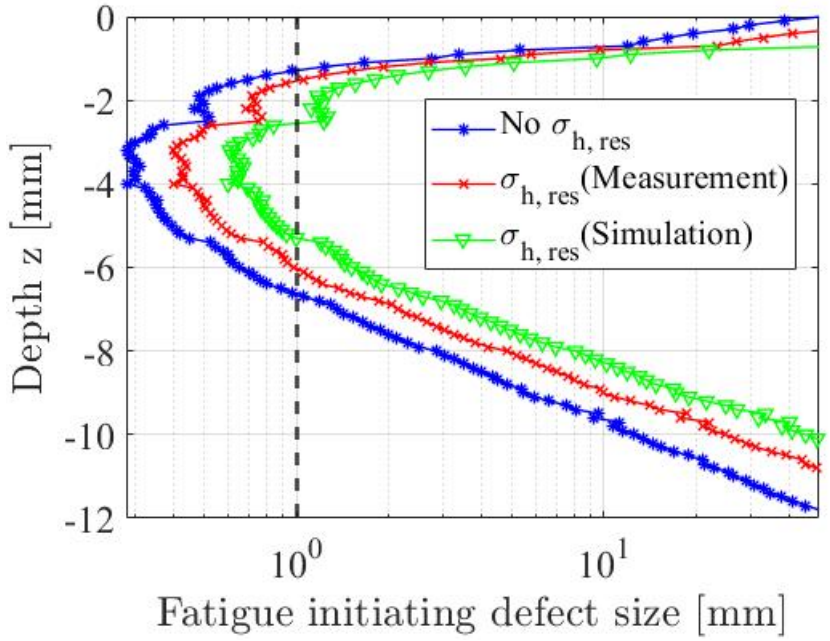

Figure 4.10: Fatigue initiating defect sizes along depth with residual stress effects

Table 4.1: Residual stress effects on the critical defect size, $d_{\mathrm{FI,min}}$ and fatigue initiating defect size, d_{FI} at a depth of -6 mm

Case	No $\sigma_{\mathrm{h,\,res}}$	$\sigma_{\mathrm{h,\,res}}$ (Measurement)	$\sigma_{\mathrm{h,\,res}}$ (Simulation)
$d_{\mathrm{FI,min}}$	0.28 mm	0.40 mm	0.60 mm
d_{FI} at -6 mm	0.65 mm	0.98 mm	1.50 mm

4.2.3 Sensitivity analysis in fatigue initiating defect sizes

The defect size analysis using equation (3.1) depends on two fatigue properties of the wheel material, (1) non-detrimental defect size, d_o, and (2) equivalent Dang Van fatigue limit, σ_{eDV}. The d_o proportionally determines defect sizes, d in fatigue initiating defect curves (See Figure 4.11). For instance, critical defect size, d_{min} varies from 0.60 mm to 1.2 mm, when d_o is increased from 20 μm to 40 μm, see Table 4.2.

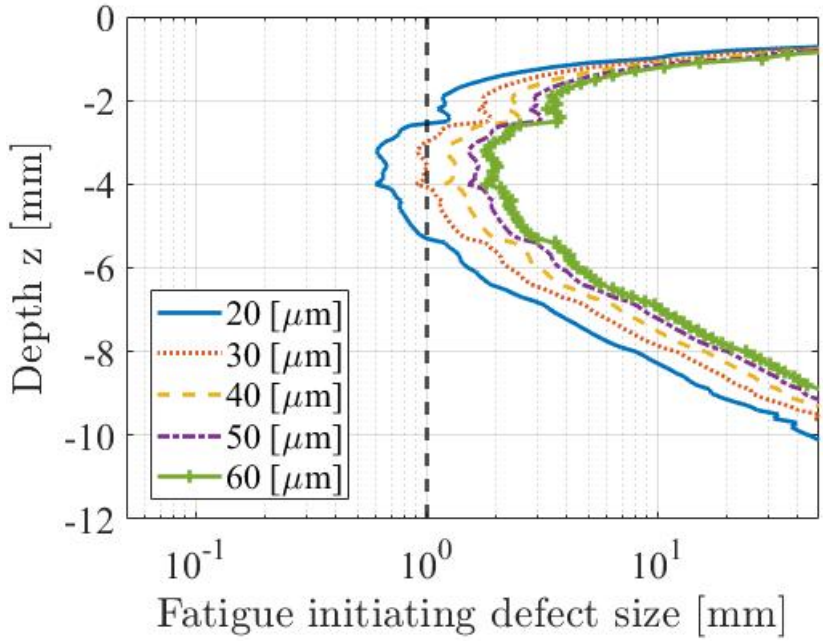

Figure 4.11: Fatigue initiating defect sizes along depth with different non-detrimental defect size, d_o

Referring to the fact that the grain size of wheel materials empirically ranges from 42 μm to 55 μm [4], the non-detrimental defect size, d_o can be roughly estimated. The critical defect size, $d_{\mathrm{FI,min}}$ is around 1.2 mm for d_o = 40 μm, which is comparable to results in [18]. Therefore, d_o ranging from 40 μm to 50 μm produces reasonable fatigue-initiating defect sizes.

Table 4.2: Critical defect size, $d_{\mathrm{FI,min}}$ and defect size at depth of -6 mm, $d_{\text{-6 mm}}$ with different non-detrimental defect size, d_o

Case, d_o	20 μm	30 μm	40 μm	50 μm	60 μm
$d_{\mathrm{FI,min}}$	0.6 mm	0.9 mm	1.2 mm	1.5 mm	1.8 mm
d_{FI} at -6 mm	1.5 mm	2.3 mm	3.0 mm	3.8 mm	4.5 mm

In addition, fatigue limit, σ_{eDV} also determines fatigue-initiating defect size, see Figure 4.12. The critical defect size is more sensitive to the magnitude of the σ_{eDV}. For example, the critical defect size, d_{min} varies from 0.29 mm to 0.58 mm, when σ_{eDV} only increases from 320 to 360 MPa, see Table 4.3. Apparently, the critical defect size analysis is highly dependent on σ_{eDV}. There have been many fatigue tests performed to precisely estimate multiaxial fatigue strength of railway wheel steels, leading to reduced uncertainty in σ_{eDV} [4], and [19]. In that sense, it is a less uncertain parameter than d_o

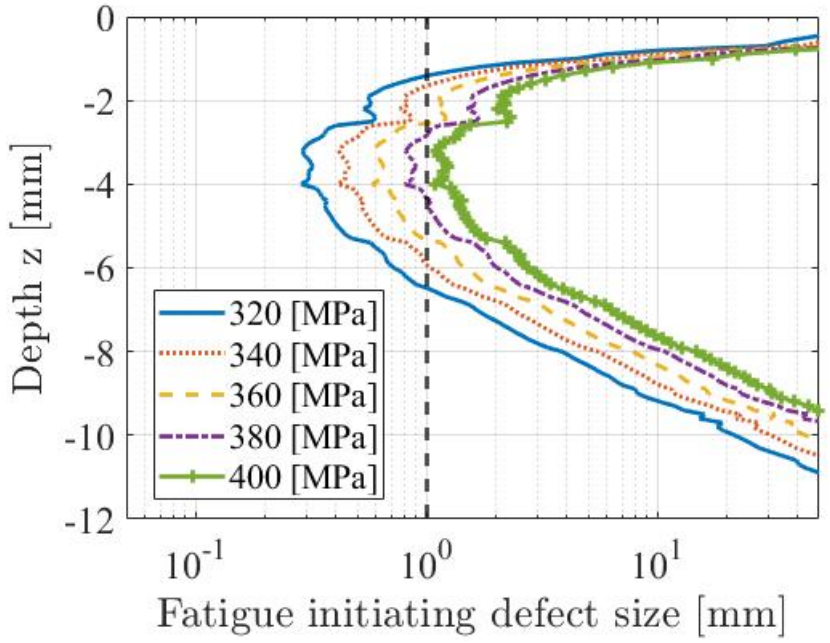

Figure 4.12: Fatigue initiating defect sizes along depth with different equivalent Dang Van fatigue limits, σ_{eDV}

Table 4.3: Critical defect size, $d_{\text{FI,min}}$ and defect size at depth of -6 mm, $d_{\text{-6 mm}}$ with different equivalent Dang Van fatigue limits, σ_{eDV}

Case, σ_{eDV}	320 MPa	340 MPa	360 MPa	380 MPa	400 MPa
$d_{\text{FI,min}}$	0.29 mm	0.41 mm	0.58 mm	0.80 mm	1.1 mm
d_{FI} at -6 mm	0.72 mm	1.0 mm	1.5 mm	2.0 mm	2.8 mm

4.3 Wheel impact load detector measurements

The analysis employs the contact force measurements of trailer wheels from wheel impact load detectors (WILD) installed in Dammstorp (near Malmö) in Sweden, see Figure 3.3. The WILDs detected contact force data during irregular periods from 2 to 5 times per month. Note that the uncertainty in wheel load detector data is not considered in this study.

4.3.1 Raw data

Figure 4.13 plots the peak force measurements from the X2 trailer wheels passing Dammstorp. The wheel on axle 4 showed an abnormal peak force, 154 kN close to the end of measurements. The right wheel on axle 4 was found to be severely defective by SJ AB. In this study, peak force measurements except for the right wheel on axle 4 are employed for extreme load predictions.

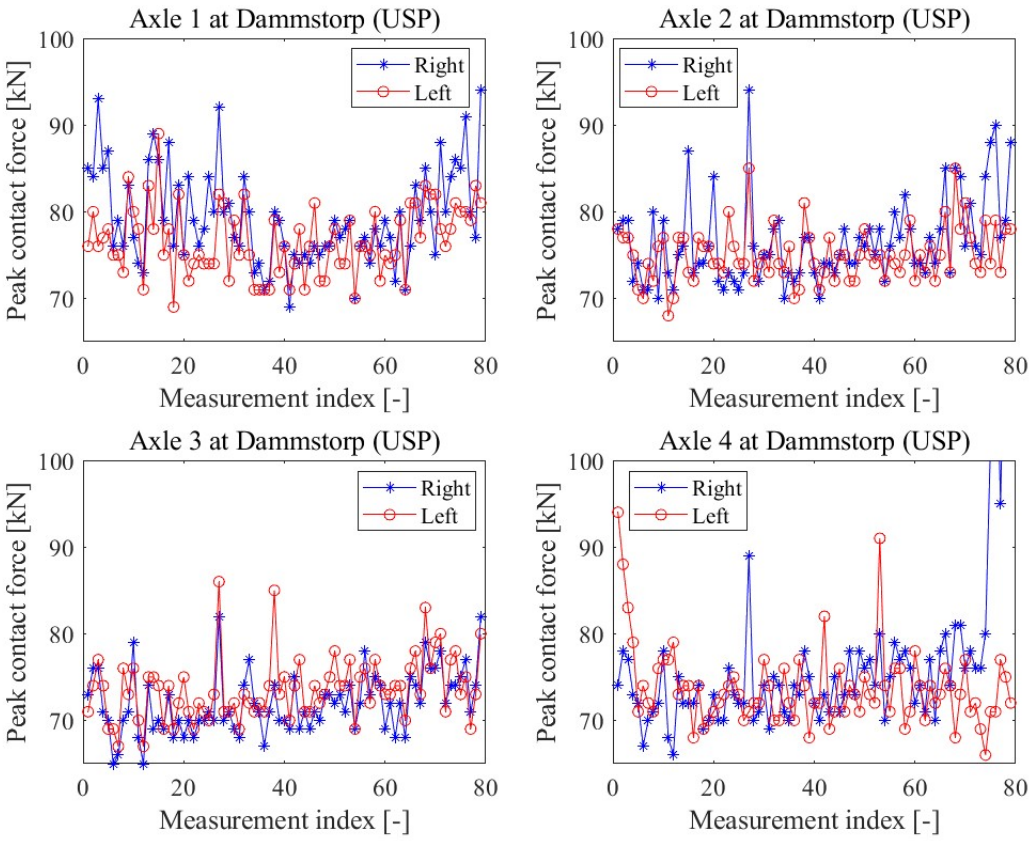

Figure 4.13: Peak force measurements of trailer wheels from WILD at Dammstorp. The peak force of defective wheel on axle 4 (right wheel) reached over 150 kN at the end.

4.3.2 Data fitting to Gumbel distribution

Gumbel is known as useful distribution to fit data acquired with long measurement intervals such as on a monthly or yearly basis. The WILDs have measured contact forces two or five times per month. The thesis selected the Gumbel distribution to fit WILD measurements and predicted extreme loads. Figure 4.14 visually displays how much the WILD measurements follow the Gumbel distribution.

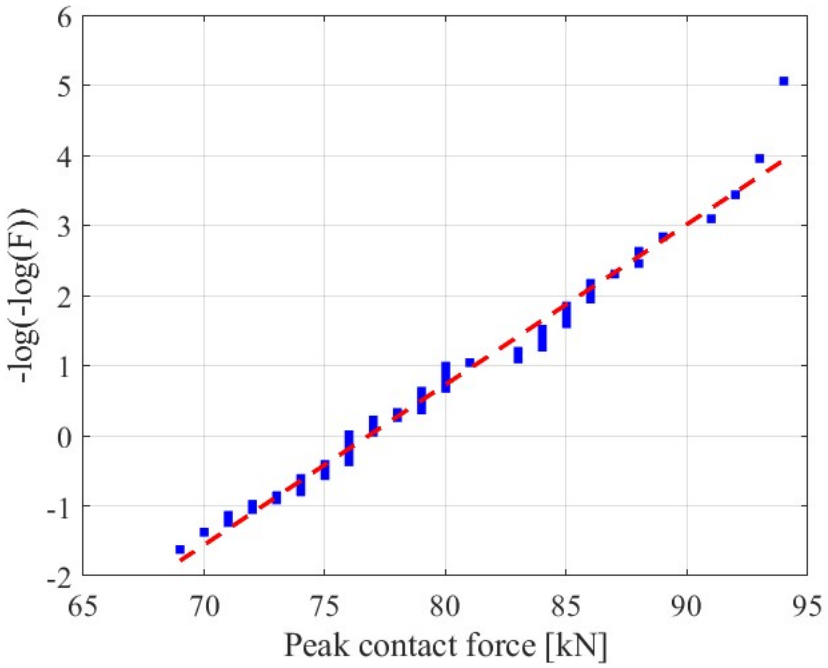

Figure 4.14: Gumbel probability plot of the trailer wheels (Right wheel on axle 1) peak force measurements from WILD at Dammstorp

Since the WILDs have measured contact forces on a monthly basis, it can be assumed that each sample in the measurements is independent. Figure 4.15 supports the independent assumption by showing low autocorrelation, − correlation of each sample with a delayed copy of itself. The maximum likelihood method is useful to fit independently distributed samples into certain distribution and derive estimates.

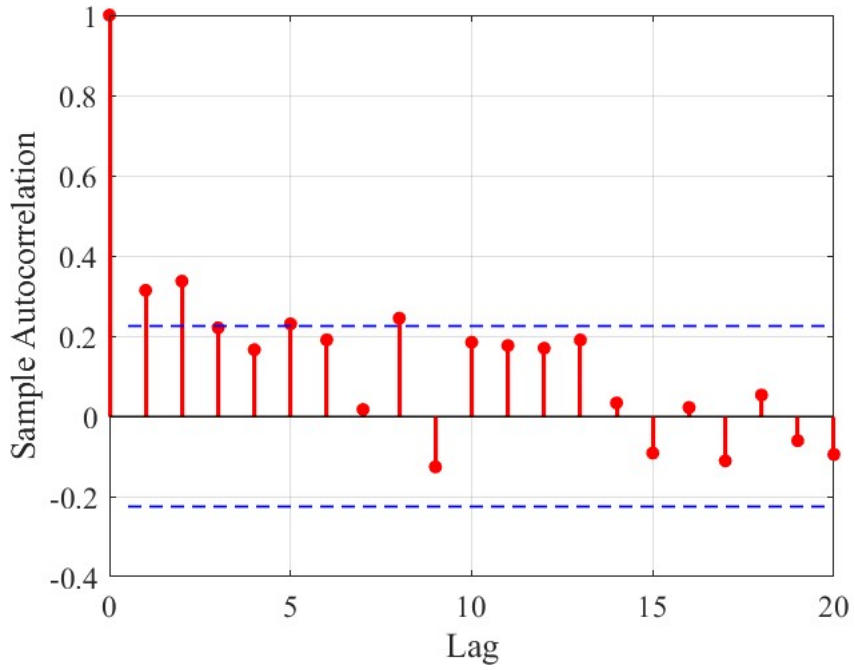

Figure 4.15: Auto correlation of the trailer wheels (Right wheel on axle 1) peak force measurements from WILDs at Dammstorp

Assuming that peak force measurements follow independent distribution, it can fit the measurements to the Gumbel distribution by using the maximum likelihood method [20]. There are two parameters for fitting measurements to Gumbel distribution, $\hat{\sigma}$ and $\hat{\mu}$ (See equation (4.1)). Table 4.4 lists parameter estimates using the maximum likelihood method with peak and mean force measurements.

$$\hat{\sigma} = \bar{x} - \frac{\sum_{i=1}^{n} x_i e^{-\frac{x_i}{\sigma}}}{\sum_{i=1}^{n} e^{-\frac{x_i}{\sigma}}}, \qquad \hat{\mu} = -\hat{\sigma} \ln\left(\frac{1}{n}\sum_{i=1}^{n} e^{-\frac{x_i}{\hat{\sigma}}}\right) \tag{4.1}$$

Table 4.4: Parameter estimates of Gumbel distribution with peak force measurements at Dammstorp (Unit: kN)

Wheel positions	$\hat{\sigma}$	$\hat{\mu}$
Right (Axle 1)	4.5	76.8
Left (Axle 1)	3.5	74.7
Right (Axle 2)	3.5	74.4
Left (Axle 2)	2.7	73.6
Right (Axle 3)	3.0	70.3
Right (Axle 3)	3.0	71.9
Left (Axle 4)	3.2	71.9
Average	3.3	73.4

4.3.3 Extreme load prediction

Note however that actual contact forces between wheels and rails can be larger than indicated WILD measurements if wheel damage causes out-of-roundness. Figure 4.16 shows the exceedance probability of peak force measurements and estimation using fitting data to Gumbel distribution. The extreme peak force value which possibly occurs once in 10 years is 106.8 kN at Dammstorp, see Table 4.5.

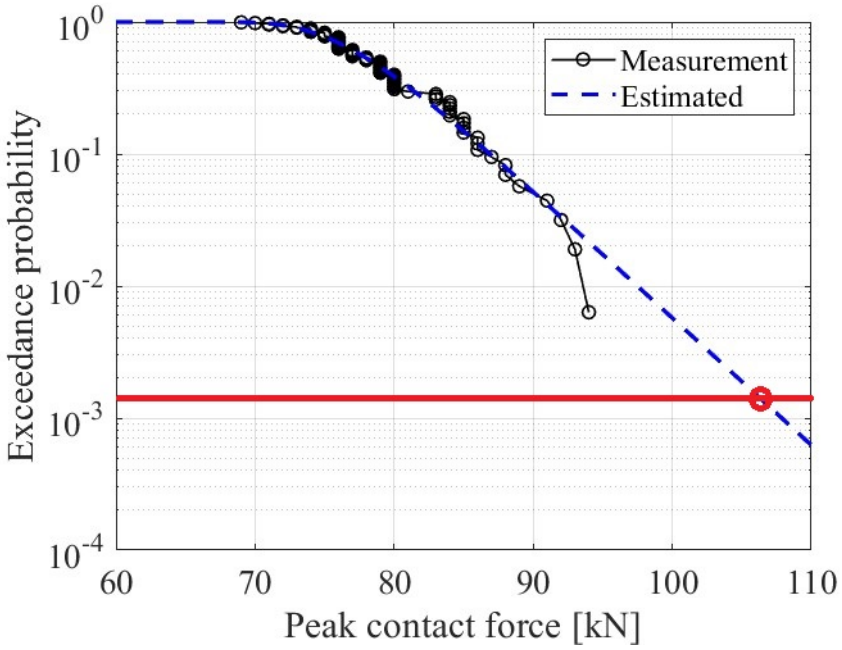

Figure 4.16: Exceedance probability plot of the trailer wheels (Right wheel on axle 1) peak force measurements from WILD at Dammstorp

Table 4.5: Parameter estimates of Gumbel distribution with peak force measurements at Dammstorp (Unit: kN)

Wheel positions	Extreme load	95 % confidence interval
Right (Axle 1)	106.8	101.2 ∼ 112.4
Left (Axle 1)	98.1	93.7 ∼ 102.5
Right (Axle 2)	97.4	93.1 ∼ 101.7
Left (Axle 2)	91.7	88.3 ∼ 95.1
Right (Axle 3)	90.3	86.6 ∼ 94.0
Right (Axle 3)	91.7	88.0 ∼ 95.4
Left (Axle 4)	92.9	88.9 ∼ 96.8

The predicted extreme loads can be applied to identify deviation levels of wheel damage from nominal states for long-term operations.

4.3.4 Defect size corresponding to loads from WILD measurements

To estimate the maximum equivalent Dang Van stress from WILD measurements, there are five steps to calculate FI_{sub} as follows. Figure 4.17 shows an example of FI_{sub} distribution peak force measurements.

- Step 1: Fit contact force measurements to Gumbel distribution
- Step 2: Generate the contact force, $\hat{p}$ from the fitted distribution.
- Step 3: Calculate contact patch semi-axes, a and b
- Step 4: Calculate $\frac{\hat{p}}{4\pi ab}$
- Step 5: Scale $\frac{\hat{p}}{4\pi ab}$ as a function of depth obtained from FE-simulation (See the Figure 4.6)
- Step 6: Add residual stress effect, $\sigma_{\text{h,res}}$ as the term of $c_{DV}\ \frac{\sigma_{\text{h,res}}}{3}$

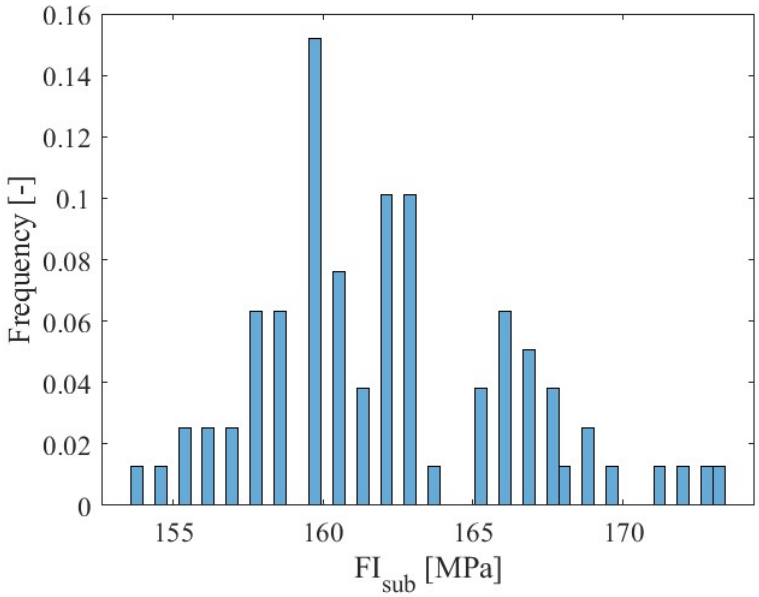

Figure 4.17: FI_{sub} distribution corresponding to peak force measurements (Right wheel on axle 1) at Dammstorp

The fitted Gumbel distribution with average parameter estimates, $\hat{\sigma} = 3.3$ kN, and $\hat{\mu} = 73.4$ kN generates FI_{sub} (See Table 4.4). The 95% of peak forces are distributed in the ranges from 69 kN to 86 kN. Based on the range, Figure 4.18 shows the maximum equivalent Dang Van stress using scaled FI_{sub} along depths.

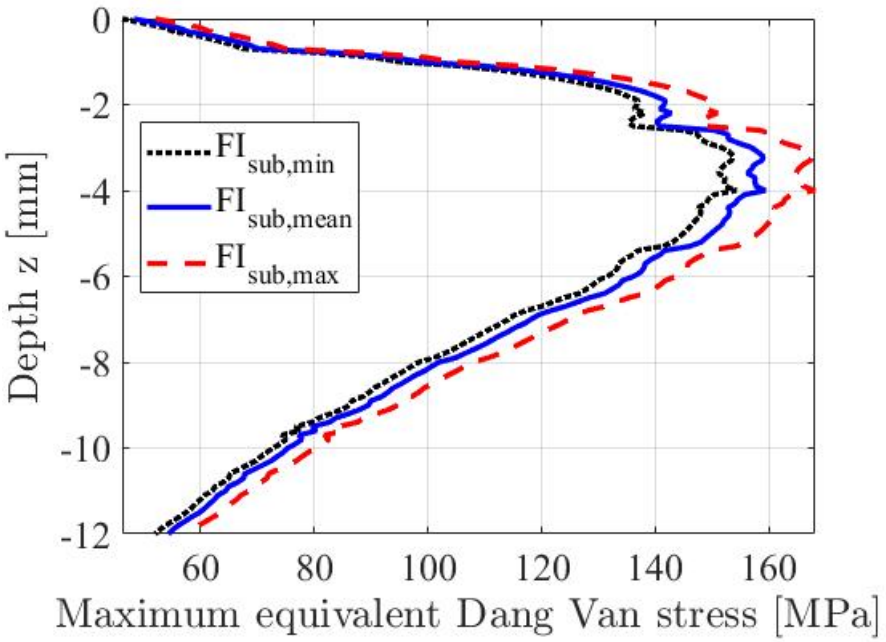

Figure 4.18: Scaled FI_{sub} along depth corresponding to peak force measurements at Dammstorp

Scaled FI_{sub} along depth can be extended to estimate fatigue initiating defect sizes, d_{FI}, see Figure 4.19. The critical defect size, $d_{\text{FI,min}}$ and the d_{FI} at depth of -6 mm individually range from 4 to 6.7 mm and 10.3 $\sim$ 17.3 mm, see Table 4.6.

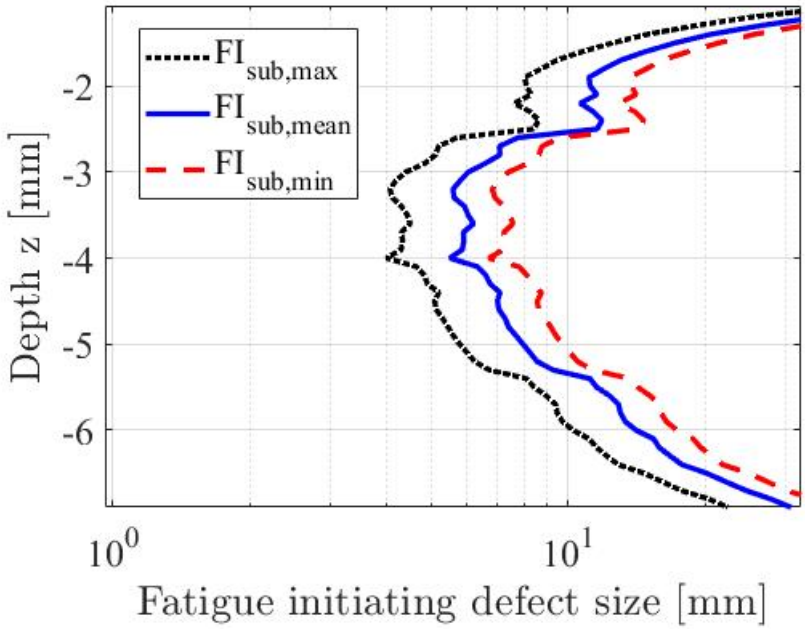

Figure 4.19: Fatigue initiating defect size, d_{FI} using scaled FI_{sub} for $d_o = 40$ μm and $\sigma_{\text{eDV}} = 362$ MPa

Table 4.6: Critical defect size, $d_{\mathrm{FI,min}}$ and defect size at depth of -6 mm, $d_{\text{-6 mm}}$ using scaled FI_{sub} along depth for $d_o = 40$ μm and $\sigma_{\mathrm{eDV}} = 362$ MPa

Case	$d_{\mathrm{FI,min}}$	d_{FI} at -6 mm
WILDs	$4 \sim 6.7$ mm	$10.3 \sim 17.3$ mm

4.4 Wheel life estimation

This section presents wheel life estimation with reduced Dang Van Wöhler curves due to material defects. The procedure for wheel life estimation includes FI_{sub} calculation by fitting WILD measurements to a Gumbel distribution. With scaled FI_{sub} in depths, the accumulated damages are obtained using the reduced Dang Van Wöhler curves.

Reduction due to depth employs semi-linear $\sigma_{\mathrm{EQ,DV}}$ distribution between depths of 3 mm to 11 mm below the surface, see Figure 4.20. For instance, the maximum $\sigma_{\mathrm{EQ,DV}}$ at the depth of 6 mm is around 86.8 % of the peak value, and $\sigma_{\mathrm{EQ,DV}}$ at the depth of 11 mm is around 46.9 % of peak value corresponding $\sigma_{\mathrm{EQ,DV}}$ around depth 3 mm, see Figure 4.20.

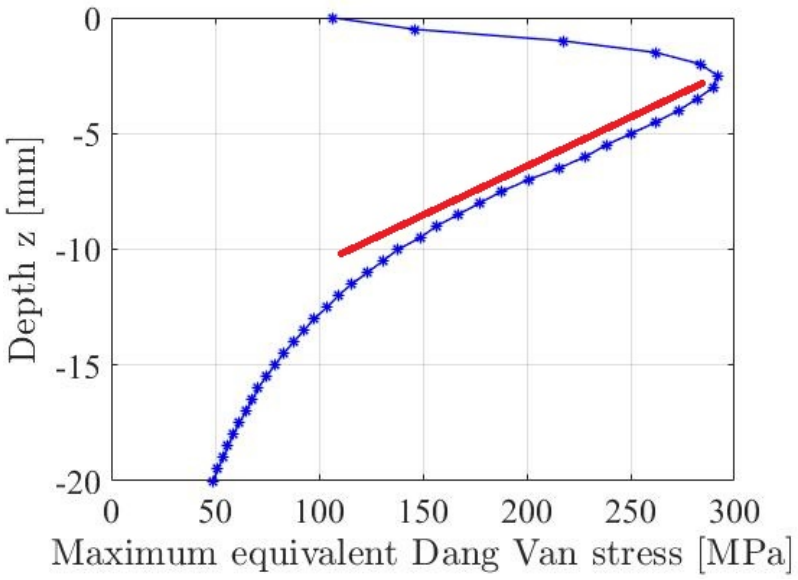

Figure 4.20: Semi-linear region in the maximum $\sigma_{\mathrm{EQ,DV}}$ from FE-simulation, compare with Figure 4.6

Defect size effects are considered in the reduced Dang Van Wöhler curves (See Figure 4.21). The reduced fatigue limit $\sigma_{\mathrm{eDV,red}}$ will determine the slope of the Dang Van Wöhler curve. In that, a larger defect size leads to a higher slope of the curve. The reduced Dang Van Wöhler curve enables us to calculate the fatigue life (or accumulated damages) for a given FI_{sub}.

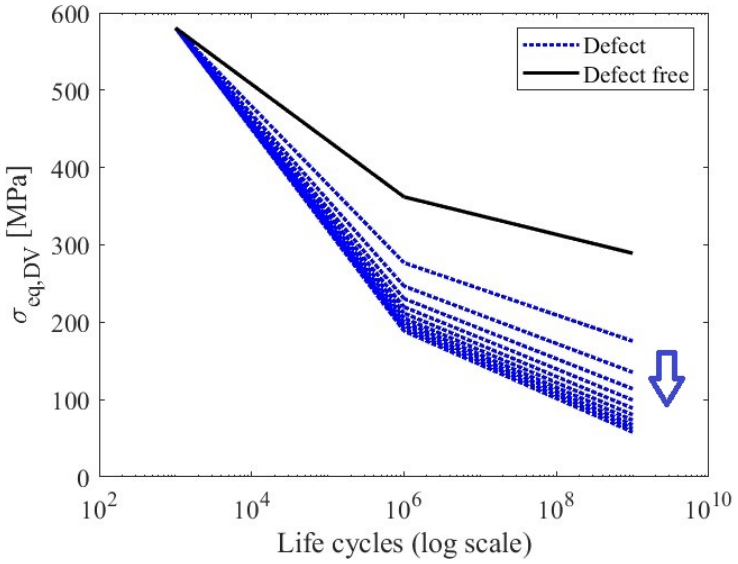

Figure 4.21: Dang Van Wöhler curve with defect sizes from 0.1 to 1 mm

Based on FI_{sub} obtained from measurements and the reduced Dang Van Wöhler curves, wheel damage is accumulated to estimate a wheel life in an iteration loop, see Table 4.7. The thesis implemented a 10 000-cycle iteration loop for wheel life estimation. Fitted Gumbel distribution with average parameter estimates from WILD measurements is employed to generate FI_{sub} for each iteration, see Table 4.4. Table 4.7 demonstrates how the size of a defect at 6 mm below the wheel tread influences the wheel life.

According to railway maintenance operators in SJ AB, trailer wheels mounted on passenger trains normally run 1 000 $\times 10^3$ km with three times wheel reprofilings. However, the wheel life estimates with empirically selected d_o = 20 μm and σ_{eDV} = 362 MPa produce unrealistically short wheel lives. Therefore, it is important to properly determine those two parameters to have reasonable wheel life estimates.

Table 4.7: Wheel life estimates at a depth of 6 mm from the peak and mean force measurements at Dammstorp for d_o = 20 μm and σ_{eDV} = 362 MPa (Unit: 10^3 km)

Defect size	Peak	Mean
0.2 mm	4 221	3 814 300
0.4 mm	333	583
0.6 mm	126	215
0.8 mm	68	115
1.0 mm	44	73

4.4.1 Sensitivity analysis in Dang Van Wöhler curves

Table 4.8 and 4.9 compare wheel life estimates with different d_o based on peak and mean force measurements. Assuming wheel materials have grain sizes around 42

$\sim$ 55 μm from [4], the d_o can be around 40 $\sim$ 60 μm. In that case, the wheel life estimates are longer than estimates with d_o = 20 μm.

Table 4.8: Wheel life estimates with different d_o at the depth of 6 mm from peak force measurements at Dammstorp for σ_{eDV} = 362 MPa (Unit: 10^3 km)

Defect size, d	d_o = 20 μm	d_o = 30 μm	d_o = 40 μm	d_o = 50 μm	d_o = 60 μm
0.2 mm	4 221	∞	∞	∞	∞
0.4 mm	333	1 036	4 229	749 999	∞
0.6 mm	126	334	734	1 434	4 217
0.8 mm	68	165	332	610	1 038
1.0 mm	44	100	191	333	542

Table 4.9: Wheel life estimates with different d_o at the depth of 6 mm from mean force measurements at Dammstorp for σ_{eDV} = 362 MPa (Unit: 10^3 km)

Defect size, d	d_o = 20 μm	d_o = 30 μm	d_o = 40 μm	d_o = 50 μm	d_o = 60 μm
0.2 mm	3 814 300	∞	∞	∞	∞
0.4 mm	583	1 857	∞	∞	∞
0.6 mm	215	583	1 301	3 426	3 689 600
0.8 mm	115	283	583	1 087	1 858
1.0 mm	73	170	330	582	960

This section also compares wheel life estimates with different fatigue limit, σ_{eDV}. The Tables 4.10 and 4.11 compare wheel life esitmates with σ_{eDV} ranging from 320 $\sim$ 400 MPa. It is found that a higher fatigue limit leads to obtaining longer wheel life estimates overall. However, wheel life estimates still remained much shorter than expected running distances with small d_o = 20 μm. For instance, wheel life estimates for the case of a 1 mm defect were shorter than 150 $\times$ 10^3 km with σ_{eDV} ranging from 360 to 380 MPa.

Table 4.10: Wheel life estimates with different equivalent Dang Van fatigue limits, σ_{eDV} at the depth of 6 mm from peak force measurements at Dammstorp for d_o = 20 μm (Unit: 10^3 km)

Defect size, d	320 MPa	340 MPa	360 MPa	380 MPa	400 MPa
0.2 mm	295	796	2 741	4 889 300	∞
0.4 mm	62	134	305	741	1 904
0.6 mm	40	57	117	250	559
0.8 mm	18	33	64	126	261
1.0 mm	13	23	41	78	154

Table 4.11: Wheel life estimates with different equivalent Dang Van fatigue limits, σ_{eDV} at the depth of 6 mm from mean force measurements at Dammstorp for d_o = 20 μm (Unit: 10^3 km)

Defect size, d	320 MPa	340 MPa	360 MPa	380 MPa	400 MPa
0.2 mm	516	1 416	1 092 000	∞	∞
0.4 mm	104	230	534	1 316	79 290
0.6 mm	48	96	199	434	992
0.8 mm	29	55	107	217	455
1.0 mm	21	37	69	132	264

The fatigue limit cycle, N_{e} of the equivalent Dang Van Wöhler curve also influences on wheel life estimation. The N_{e} determines the knee-point of Dang Van Wöhler curves. The slope of Dang Van Wöhler curves varies depending on N_{e} selection, see Figure 4.22. The small slope variation leads to inducing high scattered wheel life estimates, see Table 4.12 and 4.13.

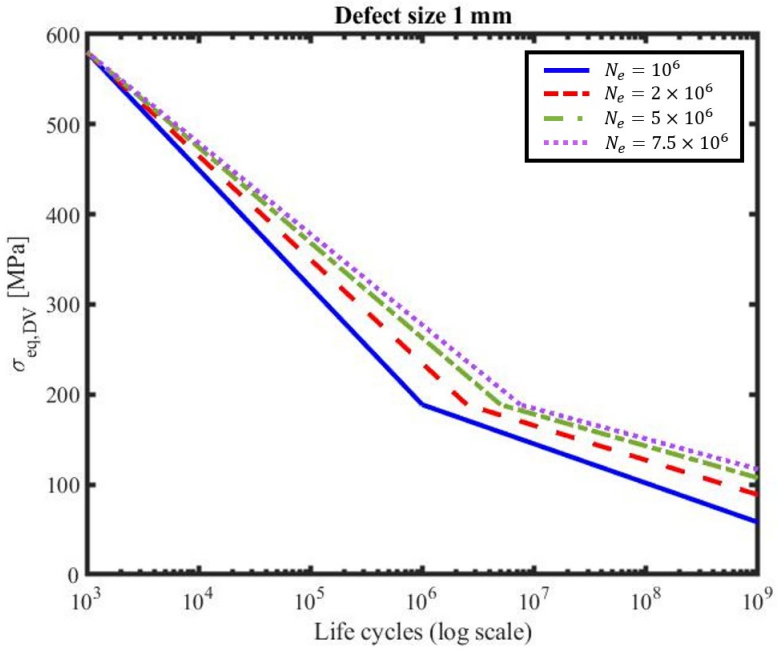

Figure 4.22: Dang Van Wöhler curve with different N_e from $1 \times 10^6 \sim 7.5 \times 10^6$ cycles

As the N_e increases, they produce larger wheel life estimates overall. However, wheel life estimates are more sensitive with larger N_{e}. For instance, wheel life for $N_{\mathrm{e}} = 10^6$ decreases by 35.3 % with increasing defect size from 0.8 mm to 1.0 mm in Table 4.12. However, the wheel life for $N_{\mathrm{e}} = 2.5 \times 10^6$ and 5.0×10^6 decreases by 39.2 % and 41.5 % respectively in same conditions.

Table 4.12: Wheel life estimates with different N_e at the depth of 6 mm from peak force measurements at Dammstorp for $d_o = 20$ μm (Unit: 10^3 km)

Defect size, d	$N_e = 10^6$	$N_e = 2.5 \times 10^6$	$N_e = 5 \times 10^6$	$N_e = 7.5 \times 10^6$
0.2 mm	4 221	∞	∞	∞
0.4 mm	333	1 566	180 120	∞
0.6 mm	126	521	1 523	6 478
0.8 mm	68	260	713	1 289
1.0 mm	44	158	417	735

Table 4.13: Wheel life estimates with different N_e at the depth of 6 mm from mean force measurements at Dammstorp for $d_o = 20$ μm (Unit: 10^3 km)

Defect size, d	$N_e = 10^6$	$N_e = 2.5 \times 10^6$	$N_e = 5 \times 10^6$	$N_e = 7.5 \times 10^6$
0.2 mm	3 814 300	∞	∞	∞
0.4 mm	583	11 185	∞	∞
0.6 mm	215	955	10 887	1 375 000
0.8 mm	115	470	1 367	3 246
1.0 mm	73	284	790	1 436

4.5 Discussion

The observation points in Chapter 4 can be summarized as follows.

- Boundary effects from finite wheel bodies and free edges due to lateral contact on subsurface-initiated rolling contact fatigue are small under elastic conditions.

- Wheel damage states can be modeled by fitting WILD measurements to Gumbel distributions. The empirically fitted distribution can be employed for extreme load prediction and wheel life estimation.

- A small defect located around 1 to 7 mm beneath the wheel tread can initiate subsurface rolling contact fatigue. The influence of small defects at deeper depths of more than 10 mm on fatigue initiation is minor. Yet, deeper defects can significantly contribute to fatigue initiation when they become close to the wheel tread after wheel reprofiling.

- Using WILD measurement load levels, a defect size less than 1 mm rarely initiates subsurface rolling contact fatigue. However, it can happen with larger external contact forces induced by severely out-of-round wheels, or rail corrugation, and accumulated wheel damages.

- Wheel life estimates are highly dependent on initial parameters: non-detrimental defect sizes, equivalent fatigue limits, and fatigue limit cycles. More empirical evidence on these parameters is required to obtain realistic wheel life estimates.

5

Conclusions and future works

The thesis investigated the influence of material defects in railway wheels on subsurface-initiated rolling contact fatigue. Firstly, it investigated finite boundary effects on subsurface stress below the wheel tread. By comparing FE-simulations with analytical solutions, boundary effects from a finite wheel body proved to be small under elastic material conditions. It also investigated the influence of lateral contact positions by moving the contact patch position toward the field side. The FE-simulation showed higher maximum level of shear stress distribution when the contact patch becomes closer to the field side. However, the boundary effects from laterally shifted contacts in realistic operating conditions also proved to be insignificant.

The thesis presented fatigue initiating defect size analysis using Murakami's theory and the Dang Van criterion. In the wheel loaded by 147 kN (axle load of around 30 tonnes), a small defect of less than 1 mm initiated fatigue at depths from 1 to 7 mm. However, the results from defect size analysis were sensitive to residual stress, non-detrimental defect size, and fatigue strengths.

Using the maximum likelihood method, measurements from wheel load detectors were fitted to Gumbel distributions. From fitted distributions, the thesis predicted the expected extreme contact loads.

Finally, the thesis estimated the fatigue life of a wheel containing a material defect at 6 mm depth below the wheel tread. It accumulated wheel damage predicted using a Dang Van equivalent Wöhler curve. It was found that the wheel life estimation could be highly influenced by small variations in non-detrimental defect sizes, equivalent fatigue limit, and fatigue limit cycles.

Future works can be listed as follows.

- Uncertainty − Both fatigue initiating defect size analysis and wheel life estimation show high sensitivity to uncertainties in parameters. It requires further research to reduce parametric uncertainties and improve the accuracy of the analysis.

- Wheel life with wheel reprofiling − The present research can extend the research question: What defect size at a depth of 11 mm would cause damage if it runs 300 $\times 10^3$ km and runs 150 $\times 10^3$ km at a depth of 6 mm after wheel turning?

- Plasticity − In FE-simulation, the present study do not take into account plastic effects on fatigue initiation. It also needs to investigate the influence of plastic deformation around rolling contact area on the fatigue initiation.

- Lateral contact forces − This thesis only considered vertical contact forces with pure rolling contacts and did not include lateral contact forces from stick and slip effects. It is also necessary to study lateral load effects on subsurface-initiated rolling contact fatigue, specially at shallow depths from 0 to 15 mm.

- Multiple defects − Results from the fatigue-initiating defect size and fatigue life estimation assumed that only single wheel defect exits in a railway wheel. However, actual material can have multiple defects close to each other. In that case, it also needs to investigate the influence of the interaction between small defects on fatigue initiation and fatigue lives.

Bibliography

[1] Andersson, E., Berg, M., Stichel, S. and Casanueva, C. (2018). *Rail Systems and Rail Vehicles: Part 1: Rail Systems*. Stockholm: KTH Royal Institute of Technology.

[2] Ekberg, A., Åkesson, B., & Kabo, E. (2014). Wheel/rail rolling contact fatigue–Probe, predict, prevent. Wear, 314(1-2), 2-12.

[3] Ekberg, A., & Marais, J. (2000). Effects of imperfections on fatigue initiation in railway wheels. Proceedings of the Institution of Mechanical Engineers, Part F: Journal of Rail and Rapid Transit, 214(1), 45-54.

[4] Ekberg, A., & Sotkovszki, P. (2001). Anisotropy and rolling contact fatigue of railway wheels. International journal of fatigue, 23(1), 29-43.

[5] Stolarski, T. A., & Tobe, S. (2000). Rolling contacts. London: Professional Engineering Publishing.

[6] Timoshenko, S., & Goodier, J. N. (1951). Theory of Elasticity: By S. Timoshenko and JN Goodier. McGraw-Hill.

[7] Lundberg, G., & Sjövall, H. (1958). Stress and deformation in elastic contacts, institute of theory of elasticity and strength of materials. In Chalmers Inst. Tech., Pub. 4, Gothenburg, Sweden.

[8] Socie, D., & Marquis, G. (1999). Multiaxial fatigue. SAE International.

[9] Dang-Van, K. (1993). Macro-micro approach in high-cycle multiaxial fatigue. ASTM Special Technical Publication, 1191, 120-120.

[10] Ekberg, A. (2000). Rolling Contact Fatigue of Railway Wheels Towards Tread Life through Numerical Modelling Considering Material Imperfections, Probabilistic Loading and Operational Data. Chalmers University of Technology.

[11] MURAKAMI, Y., TORIYAMA, T., KOYASU, Y., & NISHIDA, S. I. (1993). Effects of chemical composition of nonmetallic inclusions on fatigue strength of high strength steels. Tetsu-to-hagané, 79(6), 678-684.

[12] Ekberg, A. (2021). MULTIAXIAL FATIGUE. Gothenburg: Chalmers University of Technology.

[13] Dowling, N. E. (2020). Mechanical Behavior of Materials eBook: Global Edition. Pearson Higher Ed.

[14] Gordon, J., & Perlman, A. B. (1998, November). Estimation of residual stresses in railroad commuter car wheels following manufacture. In ASME International Mechanical Engineering Congress and Exposition (Vol. 15885, pp. 13-18). American Society of Mechanical Engineers.

[15] Demilly, F., Lonsdale, C., McCabe, T., Del Fabbro, V., Vallart, E., & Caldwell, B. (2001, September). Wheel rim residual stress measurement using ultrasonic

testing. In Proceedings of the 13th International Wheelset Congress, Rome, Italy.

[16] Trafikverket. (n.d.). Detektorer i järnvägsanläggningen. Trafikverket. Retrieved April 20, 2023, from https://bransch.trafikverket.se/for-dig-i-branschen/teknik/anlaggningsteknik/Detektorer/

[17] Brunel, F., Brunel, J. F., Dufrénoy, P., & Demilly, F. (2013). Prediction of the initial residual stresses in railway wheels induced by manufacturing. Journal of thermal stresses, 36(1), 37-55.

[18] Kato, T., Fujimura, T., Yamamoto, Y., Dedmon, S., Hiramatsu, S., Kato, H., ... & Pilch, J. (2019). Critical internal defect size for subsurface crack initiation in heavy haul car wheels. Wear, 438, 203038.

[19] Chung, C. S., & Kim, H. K. (2015). Multiaxial fatigue of a railway wheel steel. Journal of Engineering Science and Technology, 10(9), 1215-1223.

[20] Mahdi, S., & Cenac, M. (2005). Estimating Parameters of Gumbel Distribution using the Methods of Moments, probability weighted Moments and maximum likelihood. Revista de Matemática: Teoría y Aplicaciones, 12(1-2), 151-156.

[21] Ekberg, A., Kabo, E., & Andersson, H. (2002). An engineering model for prediction of rolling contact fatigue of railway wheels. Fatigue & Fracture of Engineering Materials & Structures, 25(10), 899-909.

DEPARTMENT OF SOME SUBJECT OR TECHNOLOGY
CHALMERS UNIVERSITY OF TECHNOLOGY
Gothenburg, Sweden
www.chalmers.se

CHALMERS
UNIVERSITY OF TECHNOLOGY